Article:

Bozetti, G, Kneller, B, Cronin, BT et al. (3 more authors) (2023) Lateral and temporal variations of a multi-phase coarse-grained submarine slope channel system, Upper Cretaceous Cerro Toro Formation, southern Chile. Journal of Sedimentary Research, 93 (3). pp. 161-186. ISSN 1527-1404

https://doi.org/10.2110/jsr.2022.020

Lateral and temporal variations of a multi-phase coarse-grained submarine slope channel system, Upper Cretaceous Cerro Toro Formation, southern Chile

GUILHERME BOZETTI [1,4,*], Benjamin Kneller[1], Bryan T. Cronin[2,†], Pan Li[1,§], Adam McArthur[3], Jingping Xu[4]

[1]*Department of Geology and Geophysics, University of Aberdeen, Aberdeen, United Kingdom, AB24 3UE (E-mail: bozetti@unistra.fr)*

[2]*Deep Marine Ltd, 9 North Square, Aberdeen, Scotland, United Kingdom, AB11 5DX*

[3]*School of Earth and Environment, University of Leeds, Leeds, United Kingdom, LS2 9JT*

[4]*Department of Ocean Sciences and Engineering, Southern University of Science and Technology, Shenzhen, 518055, China*

†*Present address: Tullow Oil plc, 9 Chiswick Park, 566 Chiswick High Road, London, United Kingdom, W4 5XT*

§ *Present address: Research Institute of Petroleum Exploration and Development, PetroChina, Beijing, 100083, China*

* *Present Address: Institut Terre & Environnement de Strasbourg, EOST-CNRS UMR 7063, Université de Strasbourg, Strasbourg, France*

ABSTRACT

Understanding variations in the sedimentary processes and resulting stratigraphic architecture in submarine channel systems is essential for characterizing sediment bypass and sedimentary facies distribution on submarine slopes. In the Santonian to Campanian Cerro Toro Formation, southern Chile, a coarse-grained slope system, informally known as the

Lago Sofia Member, developed in a structurally controlled environment, with complex and poorly established relationships with the surrounding mud-rich heterolithic deposits.

A detailed architectural analysis of the most continuous and best-exposed channel system in the Lago Sofia Member, the Paine C channel system, provides insights on lateral facies transitions from channel axis to margin, stacked in a multi-phase sequence of events marked by abrupt changes in facies, facies associations, and architecture.

The Paine C channel system is incised into siltstones and claystones interbedded with thin-bedded very fine sandstone, interpreted to be either channel-related overbank or unrelated background deposits. The coarse-grained deposits are divided into a lower conglomeratic unit and an upper sand-rich unit. The lower conglomeratic unit can be further subdivided into three phases: 1) highly depositional and/or aggradational, dominated by thick and laterally continuous beds of clast- to matrix-supported conglomerate, herein named transitional event deposits; 2) an intermediate phase, including deposits similar to those dominant in phase 1 but also containing abundant clast-supported conglomerates and lenticular sandstones; and 3) a bypass-dominated phase, which records an architectural change into a highly amalgamated ca. 45-m-thick package composed purely of lenticular clast-supported conglomerates with local lenticular sandstones. Between the conglomeratic phases, a meter-scale package composed of interbedded thin- to medium-bedded sandstone and mudstone deposits is interpreted to drape the entire channel, indicating periods of weaker gravity flows running down the channel, with no evidence of bedload transport.

The upper sand-rich unit is divided into lower amalgamated and upper non-amalgamated phases, and represents a rapid architectural change interpreted to record an overall waning of the system. The sandstone unit laps out onto a mass-transport complex which is interpreted to have been triggered initially at the same time as major architectural change from conglomerates to sandstones.

While mindful of the fact that each system is a complete analogue only for itself, we propose a new depositional model for coarse-grained submarine channel systems, which particular characteristics can provide significant insights into architectural heterogeneity and facies transitions in channelized systems, allowing substantial improvement in subsurface facies prediction for fluid reservoirs.

INTRODUCTION

The understanding of modern submarine channel systems can offer important information about depositional processes, geometries, and lateral facies relationships (Hansen et al. 2017; Maier et al. 2019; Vendettuoli et al. 2019; Tek et al., 2021), but provide very little information on vertical stacking patterns and internal facies distribution (Morris and Normark 2000; Kane et al. 2007; Gamberi et al. 2013; Morris et al. 2016). Detailed work on continuous exposures of ancient systems at outcrop, via combinations of mapping, logging, and photomosaic interpretation, provides valuable information on facies and architecture of these channel systems, and allows the creation of two- and sometimes quasi-three-dimensional depositional models, and generation of step-by-step multiphase reconstruction of the channel fill (Hubbard et al. 2010; Hubbard et al. 2014; Li et al. 2018; Casciano et al. 2019; Kneller et al. 2020; Tek et al. 2020).

Here we present a detailed architectural analysis of a channel system (*sensu* McHargue et al. 2011), the Paine C (Crane and Lowe 2008; Bernhardt et al. 2011). It forms part of the Cretaceous Cerro Toro Formation in the Silla Syncline area, Magallanes Basin, southern Chile (Fig. 1) (Scott 1966; Winn and Dott 1979; Sohn et al. 2002; Beaubouef 2004; Crane and Lowe 2008; Hubbard et al. 2008; Bernhardt et al. 2011; Romans et al. 2011; Bozetti et al. 2018) which consists of a succession dominated by thin-bedded sandstones and mudstones that envelop packages of conglomerate and sandstone deposits, informally named the Lago

Sofia member (Crane and Lowe 2008; Lago Sofia lens of Winn and Dott 1979; Figs. 1, 2). The Magallanes Basin is interpreted to consist of a deep- to shallow-marine succession (Fig. 2), overlain by deltaic deposits (Wilson 1991; Fildani and Hessler 2005; Shultz et al. 2005; Crane and Lowe 2008; Hubbard et al. 2008; Romans et al. 2009), marking the progradation of a slope sequence onto the basin floor (Hubbard et al. 2010; Malkowski et al. 2015, 2018). The Paine C channel system was chosen for this analysis because it is the largest and most continuously exposed channel system preserved at the Silla Syncline area (Figs. 1, 2, 3). Cecioni (l957), Katz (1963), and Scott (1966) published the first accounts of the Late Cretaceous succession, describing it as a flysch sequence. Scott documented much of the small-scale sedimentology and recognized the axial sediment transport. However, in a detailed analysis of the sedimentology, Winn and Dott (1979) were the first to recognize the large-scale channel geometries, speculating on the sediment transport mechanisms, drawing comparisons between the coarse-grained channel fills and fluvial conglomerates, and suggesting three possible mechanisms for the origin of the distinctive graded diamictites (referred to herein as “transitional event deposits” or TEDs) that are characteristic of this system. Winn and Dott (1979) proposed that this succession constituted a submarine channel-levee system. Devries and Lindholm (1994) expanded on this interpretation for the Silla Syncline area, providing evidence that the channels and levees were genetically linked, detailing the levee architecture and the facies changes away from the channel margin. In contrast, Coleman (2000), while also interpreting the fine-grained, thin-bedded sediments adjacent to the channel fills as levee, concluded that they were genetically unrelated and that the channel margins were essentially erosional into an older thin-bedded succession.

Beaubouef (2004) published the most comprehensive study up to that point of the uppermost of the conglomeratic bodies of the Cerro Toro Formation (Paine C) in the Silla Syncline area, focusing on the northeast margin of the channel system. He applied the hierarchical channel-systems classification of Sprague et al. (2005), recognized the southwestward offset stacking, and proposed a sequence of development for this channel system in which the levees developed during channel bypass, followed by erosion related to channel entrenchment or migration, then infilling of the levee relief by intra-channel facies. Barton et al. (2007) also described what they regarded as levee facies in detail, differentiating what they called inner levee (internal levee of Kane and Hodgson 2011) and outer (external) levee, and recognizing sediment waves in the external levee. Crane and Lowe (2008) and subsequently Campion et al. (2011) recognized sediment waves also in what Barton et al. (2007) considered to be internal levee (*sensu* Kane and Hodgson 2011), i.e., within the channel belt bounded by the external levees. Crane and Lowe (2008, 2009) undertook a more detailed architectural analysis and mapping that included both margins of the channel system, examining in detail the surfaces that separated the several phases of channel-fill aggradation. They concluded that the thin-bedded fine-grained rocks adjacent to the channel belt were not levees directly related to the coarse-grained channel fills but had a more complex relationship, and that the coarse-grained channel fills were essentially erosionally confined.

Bernhardt et al. (2011) extended the mapping both geographically and stratigraphically to include all intervals of the Lago Sofia Member, and concluded that they were confined within a developing structure antecedent to the Silla Syncline (Gonzales and Aydin 2008).

The objectives of this work are: 1) to describe and synthesize the facies and facies associations recognized in the area; 2) to understand the heterogeneity of the channelized deposits and how they vary laterally and vertically; 3) to produce a well-constrained depositional model of the evolution of the channel system, presenting phases of channel erosion and deposition (aggradation) and their possible causes; and 4) to illustrate major differences between types of submarine channel systems, and their consequence in terms of facies prediction.

GEOLOGICAL SETTING AT THE ULTIMA ESPERANZA DISTRICT

The two-phase evolution of the southern Patagonia Basin during the Jurassic to the Cretaceous consists of an older back-arc rift basin, the Rocas Verdes Basin (RVB), and a successor retro-arc foreland basin, the Magallanes-Austral Basin (Fildani and Hessler 2005; Calderon et al. 2007; Malkowski et al. 2018). The Jurassic to Early Cretaceous Rocas Verdes Basin is associated with the breakup of Gondwana, and formed in a back-arc extensional setting (Katz 1963; Dalziel et al. 1974; De Wit and Stern 1981; Biddle et al. 1986; Wilson 1991; Calderon et al. 2007). Regional crustal extension spanned ca. 190 to 137 Ma (Stern et al. 1992; Pankhurst et al. 2000), with volcanism occurring between 154 Ma and 147 Ma (Stern and Mukasa 1992).

Magallanes Basin

During the Cenomanian-Turonian, the transition from back-arc extension to compression resulted in development of the retro-arc foreland Magallanes Basin and the onset of deep-marine clastic sedimentation, represented by deposition of the Punta Barrosa Formation, a mudstone-rich basin-floor succession with intercalated turbidite sandstone packages (Wilson 1991; Fildani et al. 2003; Fildani and Hessler 2005; Malkowski et al. 2015). Ongoing subsidence, and denudation in the source areas, are recorded by the approximately 2500 m of the Cerro Toro Formation (Fig. 2; Katz 1963; Scott 1966; Winn and Dott 1979; Calderon et a. 2007; Crane and Lowe 2008; Hubbard et al. 2008; Romans et al. 2011; Bozetti et al. 2018), dominated by thin-bedded sandstones and mudstones, and hemipelagic sediments representing the background sedimentation (Winn and Dott 1979; Beaubouef 2004). Embedded in these fine-grained deposits are packages of conglomerate-rich strata up to 400 m thick, collectively referred to informally as the Lago Sofia member (Winn and Dott 1979), interpreted as coarse-grained submarine channel fills and intervening turbidite sheet or lobe systems (Fig. 2; Katz 1963; Winn and Dott 1979; Crane and Lowe 2008; Hubbard et al. 2008; Jobe et al. 2010; Bernhardt et al. 2011; Bernhardt et al. 2012; Malkowski et al. 2015, 2018; Bozetti et al. 2018). These coarse-grained deposits form part of a diachronous channel belt that extends at least 50 km north and south from Cerro Toro (Winn and Dott 1979; Ghiglione et al. 2014; Sickman et al. 2018), and possibly from Lago Viedma in Argentina at 48° S to Cordillera Darwin in Tierra del Fuego at 54° S (Malkowski et al. 2015). In the Cerro Toro area they occur in two main outcrop belts: one approximately north-south oriented, from Laguna Amarga in the north, through Sierra del Toro, and southward to Lago Sofia (orange patches in Fig. 3A), and one northwest-southeast oriented, in the Torres del Paine National Park, known as Silla Syncline, and which is the focus of this research (red rectangle in Fig. 3A; Scott 1966; Winn and Dott 1979; Sohn et al. 2002; Beaubouef 2004; Crane and Lowe 2008; Hubbard et al. 2008; Bernhardt et al. 2011; Romans et al. 2011; Bozetti et al. 2018).

The Cerro Toro Formation is succeeded by the sandstone-rich slope channels of the Tres Pasos Formation and the overlying delta-dominated Dorotea Formation, recording a continuous shallowing of the basin due to slope progradation (Fig. 2; Katz 1963; Natland et al. 1974; Macellari et al. 1989; Armitage et al. 2009; Romans et al. 2009; Bernhardt et al. 2011; Bozetti et al. 2018; Daniels et al. 2019). With few exceptions, overall paleocurrent measurements of the Cerro Toro, Tres Pasos, and Dorotea Formations are consistently directed toward the south and southeast, parallel to the Andean mountain-front (Scott 1966; Smith,1977; Macellari et al. 1989; Fildani and Hessler 2005; Shultz et al. 2005; Crane and Lowe 2008; Hubbard et al. 2008; Romans et al. 2009; Sickman et al. 2018). Radiometric ages indicate deposition over a roughly 6 Myr time span (Bernhardt et al. 2012; Daniels et al. 2019).

Silla Syncline area and Paine C channel system

The Upper Cretaceous Cerro Toro Formation in the Silla Syncline area was first described by Scott (1966) and Winn and Dott (1979), and coarse-grained deposits of the Lago Sofia "member" were subdivided by Crane and Lowe (2008) into three informally defined "members", Pehoe, Paine, and Nordenskjold, the upper part of the Paine member (Paine C) being the focus of this research. A broadly similar division into channel-complex sets (*sensu* Sprague et al. 2002, 2005) had previously been suggested by Beaubouef (2004); Paine C corresponds to his Channel Complex Set 3.

METHODOLOGY

The data include: a detailed geological map, showing all the stratal relationships identified in the field; forty-one sedimentary-logs (ca. 1600 m in total), recording the Paine C deposits and the immediately underlying and overlying stratigraphy; and numerous photomosaic interpretations, which allow correlation between the sedimentary logs.

The geological map of the Silla Syncline area (Fig. 3) shows deposits interpreted as part of the Lago Sofia member, with all forty-one sedimentary-log locations, highlighting in rectangles some of the main photomosaic locations, and where architectural elements were defined. An interpretation of the channel pathway (continuous white line) and its axis (dashed red lines) are also illustrated.

Digital mapping combined analysis of high-resolution Google Earth® images with topographic and geological maps available in the literature (e.g., Crane and Lowe 2008; Bernhardt et al. 2011), imported to ArcGIS ArcMap, georeferenced, and used as base maps both for geographic navigation and geological orientation. Ground mapping utilized high-resolution GPS (Trimble GeoXH) to record coordinates to centimeter resolution, and geological data during the tracing of boundaries (Figs. 3, 4). The mapping benefited greatly from the effects of a catastrophic fire in 2011 that burned large areas of southern beech forest, greatly improving visibility of and access to many outcrops. The resulting field data were exported as shapefiles into ArcMap, and served as guidelines for the placement of geological boundaries on the map (Fig. 3) and for the construction of the cross sections (Fig. 4).

The sedimentary logs were measured"at 1'10 scale, and served to record in detail lateral and vertical variation of facies and facies associations, as well as the stratigraphy underlying and overlying Paine C. Roughly 1600 m of stratigraphy were recorded.

Numerous photomosaics were produced from different locations around the syncline, each using tens to hundreds of detailed pictures merged using Adobe Photoshop®. The line drawings and interpretations of the photomosaics were generated in Adobe Illustrator®.

RESULTS

A descriptive facies scheme (Table 1; Fig. 5) is presented for the Paine C and adjacent deposits. These are combined into facies associations (Fig. 6), interpreted as fundamental building blocks for the architectural elements recognized in this system (e.g., channel, overbank, splay). The Paine C channel system is composed of: i) the widespread ≤ 30-m-thick Laguna Negra Debrite (continuously exposed along the western limb and absent in the eastern limb of the syncline); (ii) a lower conglomeratic unit (Paine C1 Conglomerates; Fig. 2), which can be divided into three phases based on internal bounding surfaces and differences in facies associations (Figs. 4, 7, 8); and iii) an upper sand-rich unit (Paine C2 Sandstone; Fig. 2), with a lower amalgamated and an upper non-amalgamated phase (Figs. 4, 9). The width of the channelized deposits ranges from 3 to 4 km, the thickness of the lower conglomeratic unit is ca. 100 m, and the upper sandy unit is ca. 80 m.

Facies

The definition of facies depends on the purpose of the study (Walker 2006). In this study, a facies is defined as either on the nature of the deposits of individual flows (e.g., F5, graded sandstone to mudstone; Fig. 5), when such is identifiable; or the deposits of a series of flows, when the deposit is amalgamated and individual beds cannot be recognized (e.g., F1, conglomerates; Fig. 5). Eight descriptive facies were defined in a simplified facies scheme that groups similar deposits (Fig. 5; Table 1); comparison with previously published facies schemes for the area is given in Table 1.

Clast-Supported Conglomerate with Low Matrix Content (Facies 1)

Description: Usually inversely graded but varying from ungraded to normally graded very large pebble to large cobble clast-supported conglomerate, with 20 to 30% matrix of well-sorted granule or very coarse sandstone. Bed boundaries are not always obvious due to the high degree of amalgamation. Bed thickness is < 1 m, generally 30 to 50 cm; lateral extent is 15 to 30 m. *a*-parallel clast-imbrication is common, especially in the inversely graded beds. It normally forms gravelly lags or a stack of amalgamated deposits interbedded with subordinate lenticular sandstones, underlying other conglomeratic and sandstone facies.

Interpretation: Bedload transport by high-density turbidity currents (*sensu* Lowe 1982; Talling et al. 2012) or concentrated flows (*sensu* Mulder and Alexander 2001). Bedload transport is indicated by grain fabric (Rees 1968, 1983; Allen 1982; Postma et al. 1988) and lack of mud content (e.g., Walker 1975, 1978), possibly generated by winnowing of matrix-rich or matrix-supported deposits (Collinson and Thompson 1982). Presence as gravelly lags, especially in stacked packages, implies high sediment bypass (Stevenson et al. 2015; Kneller et al. 2020).

Clast-Supported Conglomerate with High Matrix Content (Facies 2)

Description: Organized (moderately to well-sorted, with occasional mostly *a*-parallel imbrication) pebble to cobble clast-supported conglomerates, with interstratified sand with abrupt contact with conglomerates; sandy moderately sorted matrix (25 to 40%), moderate sphericity, subangular to rounded. Bed thickness ranges from 20 cm to ca. 3 meters, and the thicker beds are laterally continuous over a few hundreds of meters.

Interpretation: Sporadic clast imbrication indicates limited bedload transport, suggesting that the gravel was deposited and buried relatively quickly. High sandy content of usually poorly-sorted matrix in clast-supported conglomerates suggests transport in a concentrated near-bed layer (Paull et al. 2018), perhaps transitional between laminar and turbulent (Kane and Pontén 2012).

Bipartite Conglomerate and Sandstone Couplet (Facies 3)

Description: Bipartite beds ≤ 1m thick formed of clast-supported, variably graded, pebble to cobble size, extraformational conglomerate, overlain by fine to very coarse sandstone, commonly with traction structures. Contact between the two parts can be diffuse, but in most cases is sharp.

Interpretation: These deposits are interpreted as representing traction transport in polydisperse flows; coarse clasts are transported along the bed by powerful sandy turbidity currents: the sand deposited over the gravel bed as the flow decelerates (Lowe 1982). Establishing single event beds or genetic links between conglomerate-sand couplets is generally not possible.

Sandstone (Facies 4)

Description: Very coarse to very fine sandstones in beds ≤ ca. 2m, with a tendency to normal grading, sometimes ending in a mudstone (Figs. 5D, 5E and 9). They form highly amalgamated packages up to 4 m or more, usually laterally continuous, but also as lenses. Dominantly structureless, but sometimes with a massive interval followed by a low-angle or horizontal parallel-laminated interval; or a trough cross-bedded or ripple cross-laminated unit; may also preserve dewatering structures Bed bases are sharp and either erosional or flat.

Interpretation: Deposition from decelerating and strongly depositional flows (Kneller and Branney 1995). Erosional bases and amalgamation suggest that the flows were either initially erosional and/or deposited on bypass surfaces of earlier flows. Original traction structures may be obscured by dewatering structures (e.g., Lowe 1975). The beds recording a gradational mudstone overlying the sandstone are interpreted a cogenetic mudstone counterpart overlying the sandstone.

Graded Sandstone and Mudstone (Facies 5)

Description: Very laterally continuous beds, typically forming normally graded couplets of sandstone and mudstone, from a few millimeters to generally < 10 cm, some with partial or rarely full Bouma sequences. Traction structures may record multiple orientations, sometimes within the same bed. Sandstones are usually < 40% of the bed.

Interpretation: Deposits of turbidity currents that overspilled from an adjacent thalweg, with individual sand–mud couplet representing one episode of overspill (*sensu* Mulder and Alexander 2001). Their character suggests that they were deposited by unsteady flows, hinting at topographic impact on flows, both within and outside the channel. This facies resembles the levee facies of Kane and Hodgson (2011).

Laminated Carbonate-Rich Siltstone and Claystone (Facies 6)

Description: Very fine-grained deposits, normally massive but sometimes with thinly laminated white or orange stripy siltstone and mudstone up to few centimeters thick.

Interpretation: Result of sediment fallout from dilute suspension in the water column, probably representing interdigitation of hemipelagic and dilute turbidity current deposits.

Debrites, Mass-Transport Deposits (MTDs) (Facies 7)

Description: Very broad spectrum, including pebbly mudstone, pebbly sandstone, matrix-supported conglomerates, debrites, slumps, and slides. Composite units may be tens of meters thick. Degree of organisation is highly variable, from slightly disturbed to completely chaotic. Intraformational rafts are common, varying from pebble size to a few meters across.

Interpretation: All are interpreted to be the product of mass failures and ensuing non-Newtonian flow, generating slightly to highly deformed remobilized deposit.

Transitional Event Deposits (TEDs) (Facies 8)

Description: Clast- to matrix-supported conglomerates, with erosional bases, inversely graded lowermost part then normally graded until the top. Matrix increases upwards (up to 90% matrix at the top). The matrix is normally graded throughout the entire deposit, but it has a large amount of clay throughout, increasing upwards. These beds are mostly overlain by sandstone grading to mudstone, frequently with a granular to pebbly lag at the contact with the matrix-supported conglomerate. Individual beds located in the lowermost part of the conglomeratic unit (Unit 1) are up to 10 to 15 m thick and can be traced across the entire 3 to 4 km of channel belt.

Interpretation: There have been a number of interpretations for these deposits, generally element of high-concentration debris flow and more dilute turbulent flow. Their origin is discussed at length below in the context of aggradational versus bypass-dominated channel systems.

Facies Associations

Based on the facies scheme, the sedimentary logs and photomosaics, eight facies associations were identified and used to interpret architectural elements (Fig. 6). They represent associations of facies that occur repeatedly across the system, following a predictable pattern, and which can be interpreted to relate to specific depositional sub-environments (e.g., channel axis, channel margin). These are summarized in the following section.

Outcrop Expression of Facies Associations

The facies associations were identified through combination of 3D visualization of the geological map (Figs. 3, 4) and the colocation of facies.

Key outcrop locations for the identification of facies associations and resulting architectural analysis are indicated in Figure 3 (colored rectangles). The red rectangle highlights areas of repetitive erosional to aggradational phases at the NE channel margin; the black rectangle highlights lateral facies change of the SW channel margin; along the southwest, between the black and red rectangles, are all the channel axis and off-axis facies association (*sensu* McHargue et al. 2011; see also Hubbard et al. 2014; Mayall and Kneller 2021); and the purple rectangle highlights thin-bedded deposits, and sandstones that lap out onto remobilized sediments.

fA1 (Channel axis; Fig. 6A)

Observations: This section focuses on two of the best-exposed channel axis sections in the Silla Syncline area. The main outcrop (section at Log GB20, Figs. 4, 8), on the western limb of the syncline, consists of: amalgamated conglomeratic deposits, dominated by facies F8 (transitional event deposits; Table 1) (Bozetti et al. 2018), interbedded with sparse packages of F1, F2, and F3 conglomerates; and some lenticular sandstones (F4; Fig. 5; Tables 1, 2). Stepped erosional bases to F8 conglomerates, frequently fluted, are common in this association (Bozetti et al. 2018).

The other channel-axis outcrop, section at Log GB23 on the southern part of the eastern limb of the syncline (Figs. 3, 10), consists of the axial part of the Paine C ca. 4 km downstream from Log GB20 (Fig. 3B), recording similar proportions of clast- to matrix-supported conglomerates (F8) and clast-supported conglomerates (F1, F2, F3), with subordinate lenticular sandstones (F4; Fig. 5). Amalgamated conglomerates, clast-supported (F1 and F2), and subordinate lenticular sandstones (F4) form units that are tens of meters thick, in which it is almost impossible to pick out individual bed boundaries. Finer-grained material is rarely preserved (Fig. 10; Table 2). However, even in the most amalgamated parts of the channel belt, the bodies of amalgamated conglomerates are separated by fine-grained deposits, usually composed of interbedded sandstone and mudstone (F5).

Interpretation: The outcrops are interpreted to represent deposits in the channel axis, for two main reasons: i) the degree of amalgamation is greatest in this central part across the outcrop belt of coarse-grained deposits (Figs. 4, 8), interpreted to represent the area where the gravity flows were most powerful; and ii) the fact that these two sections represent the deepest erosion into the underlying deposits (Figs. 8, 10), commonly used to identify and define the channel axis (e.g., Normark 1970).

There are indications of more amalgamation and erosion in the axial deposits in the SE (Log GB23, Figs. 3B, 10) than in the W (Log GB20; Fig. 8). Amongst the evidence, the underlying Laguna Negra Debrite, which is continuous and ca.15 m thick elsewhere along the western limb of the syncline (including underlying the deposits at Log GB20; Figs. 3, 4, 8), is completely absent at this location. Other evidence is the higher frequency of amalgamated clast-supported conglomerates (F1, F2; Figs. 5, 10) at Log GB23 location, especially in the upper part of the conglomeratic section, where interbedded transitional event deposits are less common (F8; Fig. 5; Table 1).

fA2 (Channel Off-Axis; Figs. 6B, C)

Observations: Amalgamated F1, F2, and F8 conglomerates, with a high percentage of bipartite conglomerate and sandstone deposits (F3) and lenticular sandstones (F4; Fig. 5; Table 1), are dominant in this facies association. Sandstones (F4) and heterolithic deposits (F5) in fA2 range from almost absent, in areas close to amalgamated conglomerates (interpreted to be channel axis; Fig. 6B), to very common in areas interpreted as close to the channel margin (fA2*; Fig. 6C), where conglomerates are absent. Beds of conglomerate transitioning laterally into sandstones, sometimes interfingering and sometimes grading, are common in this facies association, generally forming F3 (Fig. 11). The boundary between the channel axis and off-axis deposits is arbitrary (Campion et al. 2000; McHargue et al. 2011; Fildani et al. 2013; Hubbard et al. 2014, 2020), and is here defined as adjacent to the deepest erosional cut of the channel axis deposits (Fig. 6), where channel-axis conglomerates (F1, F2, F3, F8; Fig. 5; Table 1) are no longer highly amalgamated (thus preserving a relatively high proportion of lenticular sandstones), and transition laterally into amalgamated sandstones (F4), or more rarely, interbedded sandstone and mudstone (F5; Figs. 11, 12). Channel off-axis is defined as extending laterally until conglomerates (F1, F2, F3, F8) are absent, and lenticular sandstones (F4) pass laterally into heterolithic deposits (F5) via another arbitrary boundary that separates channel-off-axis (fA2*) from channel-margin facies association (fA3; Figs. 6, 8, 11, 12, Log GB1; see below).

Figures 6B and 6C (fA2) illustrate examples from two different channel off-axis sites, 6b being interpreted to be closer to the channel axis, and 6C closer to the margin (fA2*). In the Laguna Corazon section, between Log GB7 and Log GB4 (Figs. 3, 8, 11), the best exposure of this facies association records gravelly beds changing laterally into sandstone and heterolithic deposits (Fig. 11).

Interpretation: The channel off-axis is interpreted as an area in the channel where, although the flows were sufficiently competent to transport coarse sand in suspension and move gravel as bedload, they were less so (and relatively more depositional) than in the axial area. Additionally, intermittently weaker flows might have also deposited sand across the entire axis and off-axis areas, which was later eroded in the axis where flows were more competent (Figs. 11, 12).

fA3 (Channel margin; Fig. 6D)

Observations: This facies association is dominated by: thin-bedded graded sandstone to mudstone (F5), normally preserving sedimentary structures; interbedded with randomly distributed thicker sandstones (F4), usually highly structured (e.g., trough cross-bedding, parallel lamination and ripple cross-lamination), forming neither regular packages nor trends; and subordinate slumps and debrites (F7; Figs. 5, 11; Tables 1, 2). These deposits are found within the channel belt, lateral to the off-axis deposits, separated by arbitrary boundaries (Fig. 11). Outside the channel confinement (black rectangle, Fig. 3), the fA3 deposits lap onto very thin-bedded carbonate-rich silt and clay with scattered thin, very fine-grained sandstones (fA8; Fig. 4). Towards the NE channel margin, the facies transition from channel off-axis to margin is less evident, changing abruptly into the intrachannel heterolithics (fA6; Fig. 12).

A distinct trace fossil Is identified in this type of facies association, consisting of sand-filled tubes 2 to 3 cm in diameter and ca. 40 cm long (*Diplocraterion* sp., *sensu* Hubbard and Schulz 2008) connecting thicker sandstone beds through heterolithics (Fig. 6d).

Interpretation: The beginning of the channel-margin deposits is herein defined as the point beyond which conglomerates are completely absent and heterolithic (F5) packages are dominant over medium- to thick-bedded sandstones (Fig. 11; Table 2). *Diplocraterion* sp. (Hubbard and Shultz 2008) has been recognized in exhumed or firmground environments dominated by sediment bypass, and in deep-water settings is usually associated with the base of submarine channels and terraces. These deposits represent part of a feathering out of the Paine C Phase 1 channel fill, away from the channel axis (Fig. 11). Farther to the SW they appear to lap onto a composite erosional surface cutting into fine-grained sediments of the Laguna Negra Debrite and slope (Figs. 4, 11).

Submarine channel margins have been recognized in outcrop with two specific different characteristics: i) channel-margin drapes (Camacho et al. 2002; McHargue et al. 2011; Fildani et al. 2013; Hubbard et al. 2014; Li et al. 2016), commonly bioturbated, which are suggestive of slow deposition from dilute upper part or tails of turbidity currents (e.g., Walker 1975; Campion et al. 2000; Campion 2005; Camacho et al. 2002; Grecula et al. 2003;

Macauley and Hubbard 2013; Callow et al. 2014; Stevenson et al. 2014, 2015; Li et al. 2016); and ii) lateral facies transition from axial coarser-grained into a marginal fine-grained domain (Campion et al. 2000; Sullivan et al. 2000; Cronin et al. 2005; Crane and Lowe 2008; Jobe et al. 2010; Kane et al. 2010; Di Celma et al. 2011; Brunt et al. 2013; Macauley and Hubbard 2013; Li et al. 2016; Bozetti 2017), where flow expands over a larger area away from the channel thalweg (axis), becoming gradually less competent away from the axis, and therefore more depositional towards the channel margins (Kneller and McCaffrey 1999; Hubbard et al. 2014; Casciano et al. 2019). The latter is interpreted to be the dominant process in the Paine C channel system, at least in its initial phase.

fA4 (Amalgamated Sandstones; Fig. 6E)

Observations: Generally forming prominent ridges, this facies association consists of 6 to 10 m packages (Figs. 4, 6e, 9, 12) dominated by sandstones (F4), interbedded with graded sandstone to mudstone (F5; Fig. 5; Table 1). The sandstone packages are composed of amalgamated sandstone beds, usually with a granular or pebbly lag at the base, and sometimes with a thin granular and mud-clast rich horizon above each amalgamation surface (F3) (Figs. 5, 9; Tables 1, 2). Individual beds are traceable for several meters until they pinch out either due to amalgamation or simply due to impersistence, perhaps a result of erosion by nondepositional flows. Notwithstanding, amalgamated packages as a whole are laterally traceable across the entire ca. 4 km outcrop belt.

This facies association is the main component of the Paine C sand-rich unit (Paine C Phase 4), which laps onto F6 towards the SW channel margin (Figs. 3, 4), and onlaps abruptly onto a large mass-transport deposit (fA6) towards the NE channel margin (Figs. 3, 4, 13).

Interpretation: The discontinuity of the beds and abrupt nature of pinch-out suggests that the high-density turbidity currents or concentrated flows (Lowe 1982; Mulder and Alexander

2001) responsible for depositing these beds were confined within the channel belt, were sand-rich, and strongly density-stratified (Kneller and Buckee 2000; Peakall et al. 2000; McCaffrey and Kneller 2001; Stevenson et al. 2014; Li et al. 2016; Soutter et al. 2019). Given the small amount of mudstone preserved in this facies association, fine-grained sediments either overspilled out of the channel, bypassed, or were eroded away by subsequent flows (Piper and Normark 1983; Hay 1987; Straub et al. 2011; Stevenson et al. 2014, 2015), the latter being interpreted as the principal mechanism acting to produce amalgamated sandstones facies associations. The discontinuity of individual beds, continuity of the packages, and lack of sandstones observed in the overbank areas suggests that the flows transporting these sediments into the system during this phase were restricted to the channel belt.

fA5 (Non-Amalgamated Sandstones; Fig. 6F)

Observations: This facies association is composed mostly of separate beds of sandstone (F4) generally 30 to 50 cm thick, with rare beds > 1 m, mostly in the lower part of occurrences of this facies association. Rarely a granular to pebbly interval is encountered at the base of each sandstone bed (F3), as well as thin discontinuous intervals of debrite (F7) (Figs. 5, 9; Tables 1, 2). The mudstone part of the bed usually varies in proportion to the thickness of the underlying sandstone, and is commonly thicker than the sandstone. 20 to 50 cm of erosion is observed at the bottom of some of the coarser sandstone beds, though bed amalgamation is much less common than in the amalgamated-sandstones facies association (fA4). The beds are normally graded throughout, but do not necessarily preserve all five Bouma divisions (*Ta* to *Te*) mentioned in Table 1. Some divisions may be randomly missing (e.g., missing parallel-laminated sandstone –– Bouma *Tb* –– in the middle of the bed). These are interbedded with 1 to 3 m thick deposits of heterolithics (F5), or thinly laminated carbonate-rich silt and clay (F6; Figs. 5, 9; Tables 1, 2). The thickness of sections of this facies association typically ranges from 6 to 12 m, and is composed of beds that are laterally relatively continuous but not traceable across the entire outcrop belt (Fig. 9).

This facies association is the main component of Paine C Phase 5 (Fig. 9), whose onlap is generally poorly exposed, but where preserved, the mudstone beds appear to wedge out as they onlap the MTD, not ending abruptly but forming a drape.

Interpretation: The non-amalgamated sandstones facies association is interpreted as deposits of concentrated or high-density flows, interbedded with muds indicating periods with deposition from smaller and less competent turbidity flows (e.g., Mutti 1992; poorly exposed gray areas in Fig. 9).

The preservation of thick mudstone caps in the turbidite sandstone beds indicates lack of sediment bypass and/or erosion in the system, and trapping of the mud where flows were confined to the channel belt. The discontinuity of the beds suggests that the flows that deposited this unit were smaller than the flows that deposited the amalgamated sandstones, and did not spread across the entire channel belt. The lateral sandstone-to-mudstone pinch-outs onto the adjacent sloping upper surface of the MTC suggests that the flows were substantially muddier than those that deposited the amalgamated facies associations (Kneller and McCaffrey 1999; Smith and Joseph 2004; Patacci et al. 2015; Li et al. 2016).

fA6 (Terrace and/or Internal Levee Deposits; Fig 6G)

Observations: Heterolithic deposits are dominant, formed by graded sandstone to mudstone generally varying from 5 to 40 cm in thicknesses (F5), often interbedded with thicker sandstones (F4; Figs. 5, 12; Tables 1, 2), with individual beds usually ranging from 25 to 80 cm thick. The sandstone beds are mostly medium- to coarse-grained and laterally persistent for hundreds of meters. The beds commonly have sedimentary structures, with ripple cross-lamination being dominant, but also with parallel lamination, and a crude lamination marked by centimeter-scale alternations between medium- and coarse-grained or occasionally granular sand. Multiple paleocurrent directions have been measured in some ripple cross-laminated sandstones. The same deposits form lenticular sandstone-rich beds in mud-dominated deposits.

Interpretation: Lenticular deposits have been described as sediment waves (Campion et al., 2011) However, these deposits are herein interpreted as intrachannel-belt heterolithics, deposited either as terrace or internal levee (*sensu* Kane and Hodgson 2011, Hansen et al. 2015) (Fig. 5). The interbedded sandstone and mudstone occur immediately laterally adjacent to the conglomerates (channel off-axis) at the NE channel margin (red rectangle in Figs. 3, 4, 8, and 12; Logs GB22, GB40), and are broadly contemporaneous to at least some of the coarse-grained channel fill, which forms repeated cycles of coarse-grained channel incision and aggradation, laterally bounded by this fine-grained association (Fig. 12). Multiple paleocurrent directions observed in single rippled sandstone beds are interpreted to represent flow interaction with channel-belt margins (Kneller et al. 1991; Kneller 1995).

fA7 (Confined Mass-Transport Complex; Fig. 6H)

Observations: A large (ca. 80 m thick) mass-transport complex (MTC) (Figs. 5, 6), located on the east limb of the syncline (purple rectangle, Fig. 3), contains deformed deposits with various degree of disaggregation and variable composition. No extraformational clasts were encountered in this facies association. Different mass transport deposits (MTDs) were observed, based primarily on the type of the incorporated sediments (different facies type) and their degree of disaggregation. At least three MTDs were identified comprising this MTC (Fig. 13), based mostly on descriptions in sedimentary Log GB39.

Interpretation: The MTC represents a series of different mass-transport deposits, interpreted based on composition and different degree of disruption. When relatively well preserved, the MTDs appear identical to the laterally adjacent *in situ* F6 deposits, immediately outside the channel belt (Fig. 4), which are therefore interpreted as their protolith. These fine-grained deposits in the MTD 1, similarly to the adjacent F6 unit, preserve a horizon 50 cm to 1 m thick with numerous sand-filled burrows both vertical and horizontal. fA4 and fA5 deposits of the Paine C Phase 4 and 5 (Fig. 6H) lap out onto this channelized MTC (Fig. 13).

fA8 (Slope or External Levee Deposits; Fig. 6I)

Observations: This facies association occurs adjacent to the Paine C channel belt, and it is composed of thin-bedded carbonate-rich siltstone and claystone, with infrequent fine- to very fine-grained thin-bedded sandstones, with a high proportion of sand-starved sections dominated by carbonate-rich muddy intervals (Fig. 6I). Sand content is less than 10% overall (Table 2).

Interpretation: On the basis of data presented here, at least two interpretations are possible for the deposits outside the channel belt:

- this was a topographic high adjacent to the channel belt, containing a large proportion of carbonate-rich22emipelagitese-dominated, interbedded with thin fine-grained siliciclastic deposits generated by sparse larger flows that spilled out of the channel margin. This represented a steep erosional channel margin, which collapsed in a series of events, generating a mass-transport complex (Fig. 13);
- alternatively, the topographic high that generated the MTC was a levee crest, immediately adjacent to the channel. In this interpretation however, the thin-bedded deposits are interpreted to be the product of flow stripping (Hampton 1972) and overspill of the finer-grained sediments in suspension in the upper parts of the turbidity currents flowing down this channel. Fine-grained sandstone with common sedimentary structures (ripple cross-lamination) would be expected to support this interpretation.

These issues are the subject of ongoing work and will be dealt with in subsequent publications.

Stratigraphic Organization

Underlying the conglomeratic units of the Paine C channel system (and possibly associated with it) is the mud-dominated deposit of the ≤ 30 m thick Laguna Negra Debrite (LND). The base of the LND erodes up to at least 1 meter into the underlying deposits. The lowermost part of the LND consists of a ≤ 120 cm (usually 30 to 80 cm) inversely to normally graded clast-supported conglomerate, with large pebbles to large cobbles (16 to 128 mm) of mostly extraformational crystalline material; there is a continuous upwards decrease in the amount and size of extra-formational clasts and increase in mud content of the matrix. Small mudstone, sandstone, and heterolithic clasts are also encountered in the clast-supported conglomerate part of the deposit, and large rafts of the same material are found usually in the middle to upper part of the bed. The LND becomes thicker and muddier with rather patchy outcrops as one moves outwards from the axis of the overlying Paine C channel towards the channel margins, especially the SW channel margin (Figs. 4, 8). This deposit was previously interpreted as “choking” the underlying Paine B channel, leveling out the local topography (Crane and Lowe 2008). Nonetheless, observations described herein, especially the termination of the bed toward the SW and the similarities in clasts with the overlying Paine C conglomerates, support the hypothesis that the LND is associated with the initiation of deposition of the Paine C channel system.

The overlying ca. 180-m-thick Paine C channel system fill overall grades upward from conglomerates to sandstones. Its stratigraphy can be divided into five units, referred to here as Phases 1 to 5, based on detailed architectural analysis and the distribution of the facies associations.

Phase 1

The thickness of this unit varies laterally between 5 and 30 meters (15 to 20 m in general), and it is erosive into the underlying stratigraphy, which on the western limb of the syncline is the Laguna Negra Debrite (Figs. 4, 8, 11, 12), and on the eastern limb is the underlying sheet sandstone system, the Paine A sandstones (e.g., Bernhardt et al. 2011) (Figs. 2, 4, 10). Phase 1 is composed dominantly of the following:

- In its axial section (fA1), transitional event-deposit conglomerates (F8; Figs. 5i, 5j), confined to the conglomeratic channel belt (Beauboeuf 2004; cf Winn and Dott 1979) with subordinate clast-supported conglomerates with low to high matrix content (F1 and F2 respectively; Fig. 5A, 5B), bipartite conglomerate and sandstone couplets (F3; Fig. 5C), and lenticular sandstones (F4; Figs. 5D, 5E);
- In the channel off-axis (fA2/2*), a combination of similar proportions of clast-supported conglomerate (F1, F2; Figs. 5A, 5B) and bipartite conglomerate and sandstone couplets (F3; Fig. 5C), sandstones (F4; Figs. 5D, 5E), and graded sandstone to mudstone (F5, Fig. 5F), with the proportion of coarse-grained deposits (F1 to F4) decreasing towards the margin (fA2*);
- On the channel margin (fA3), dominantly interbedded sandstones (F4; Figs. 5D, 5E) and graded sandstone to mudstone (F5; Fig. 5F).
- On the SW channel margin these deposits transition laterally from conglomeratic to sand-dominated to mud-dominated and finally to a complete pinch-out (Scott 1966; Winn and Dott 1979; Crane and Lowe 2008; Bernhardt et al. 2011) (Figs. 8, 11).
- Towards the NE channel margin, Phase 1 consists of conglomerate-dominated deposits, less amalgamated than in the axial section, which end abruptly at the park highway (Figs. 3, 4), as recorded in the Log GB40 (Figs. 8, 12).
- Between Phases 1 and 2, a package of ca. 1 m of interbedded thin- to medium-bedded sandstone and mudstone is present across most of the outcrop belt, absent only where phases 1 and 2 are amalgamated (Figs. 8, 11; see Bozetti 2017, Fig. 7.7 for detail).

Phase 2:

Phase 2 varies laterally between 20 and 40 meters in thickness (25 to 35 m in general) (Figs. 4, 8). It erodes into the Phase 1, and is composed of clast-supported conglomerates with low and high matrix content (F1 and F2 respectively; Fig. 5A, 5B), bipartite conglomerate and sandstone couplet (F3; Fig. 5C), lenticular sandstones (F4; Figs. 5D, 5E), and transitional event-deposit conglomerates (F8; Figs. 5I, 5J), following no obvious vertical trend. Amalgamation decreases away from channel axis, but lateral facies trends are less obvious than those observed in Phase 1 (Fig. 8). There appears to be an increase in transitional event deposit conglomerates towards the SW channel margin, where Phase 2 ends abruptly at a surface laterally separating the coarse-grained deposits from poorly exposed interbedded very fine-grained sandstone and mudstone (Figs. 8, 11); towards the NE channel margin, composed dominantly of fA3 and subordinate fA2, a series of erosional and aggradational features are observed (Figs. 4, 8, 12) (Crane and Lowe 2008; Bernhardt et al. 2011), the facies become less amalgamated, with an alternating higher proportion of sandstones (fA3) and conglomerates (fA2; Fig. 12). At the NE channel margin (Log GB22 location), a package of sandstones and mudstones (fA6) is observed lateral to Phase 2, following a fining- and thinning-upwards trend (Fig. 12). In this package, some of the sandstones have parallel lamination and ripple cross-lamination, sometimes recording multiple paleocurrents; most of the thicker sandstones have dewatering structures. Soft-sediment deformation (e.g., folded sandstone beds) and meter-thick slide blocks overlain by healing sandstones are also observed in this package (Bozetti 2017). Between Phases 2 and 3, similarly to Phases 1 and 2, there is a ca. 1-m-thick package of interbedded thin- to medium-bedded sandstone and mudstone recorded across most of channel belt.

Phase 3:

Phase 3 ranges between 35 and 55 meters (40 to 50 m in general), is highly erosive into the most axial parts of Phase 2, and it is absent towards the channel margins (Figs. 4, 8, 10);

on the NE margin due to pinch-out, and on the SW margin due to modern erosion. It is composed dominantly of clast-supported conglomerates with low- and high-matrix content (F1, F2; Figs. 5A, 5B), lesser bipartite conglomerate and sandstone couplets (F3; Fig. 5C), and lenticular sandstones (F4; Figs. 5D, 5E). In the axial part Phase 3 is easily identified, but towards the NE channel margin, and especially the SW channel margin, the correlations are problematic due to the structure of the syncline and lack of outcrop continuity.

The confined MTD on the northeast channel margin overlies the interbedded sandstone and mudstone deposits of Phase 2, and consists of at least three distinct units, differentiated based mainly on degree of disruption and content:

- MTD 1: the remobilized material consists of moderately disrupted strata, with sub angular blocks of the protolith ranging between 1 and 4 meters, consisting, where identifiable, of material very similar to the undeformed heavily bioturbated, interbedded very fine carbonate-rich very-fine sandstone and mudstone deposits encountered outside the channel (F6; Fig. 5G; Table 1);
- MTD 2: various types of blocks can be identified in a very disaggregated state, with individual blocks almost unrecognizable. They include 50 cm to 10 m blocks of interbedded carbonate-rich very fine sandstone and mudstone deposits (F5), and 20 cm to 20 m rounded to angular blocks of sandstone (F3), seemingly increasing in size and abundance towards the top of this MTD; and
- MTD 3: composed dominantly of interbedded carbonate-rich very fine sandstone and mudstone deposits (F5), with some blocks of interbedded fine- to medium-grained sandstone and mudstone (F4), all substantially less disaggregated than the underlying MTD.

Phase 4:

This consists dominantly of ca. 30 m of highly amalgamated sandstone facies association (fA4; Figs. 6E, 9), in which the lowermost sandstone beds interdigitate with some clast-supported conglomerate or pebbly sandstone beds, occasionally cross-stratified (F1 and F2; Figs. 5A, 5B, 9), sometimes with bipartite conglomerate and sandstone couplets (F3; Fig. 5C), or a lower gravelly lag in the sandstone deposits (F4; Figs. 5D, 5E); and less common non-amalgamated facies association (fA5; Figs. 6F, 9). This phase is dominated by fA4 in the lowermost part of the section, and fA5 towards the top (Fig. 6), recording a fining- and thinning-upwards sequence (Figs. 9, 12, 13). Sedimentary structures such as parallel lamination are common in the upper part of the beds, as well as dewatering structures (Fig. 6E). Amalgamation of the Phase 4 sandstones decreases towards the channel-belt margins. Towards the NE channel margin, they lap out abruptly onto the mass-transport complex ca. 50 to 60 meters thick (Fig. 13),

Towards the SW channel margin, where the sandstones are highly structured, preserving trough cross-bedding and low-angle cross-bedding, they pinch out onto an abrupt boundary that separates the sandstone deposits (F4; Figs. 5D, 5E) from poorly exposed interbedded very fine-grained sandstone and mudstone (Fig. 5F). Separating the amalgamated and the non-amalgamated phases is a ca. 3 m transitional event deposit (F8; Figs. 5I, 5J; Table 1), composed dominantly (ca. 50 to 60%) of the debritic matrix-supported portion. Small-scale (ca. 1 to 2 m) ponding of the overlying Phase 5 sandstones is observed on the relief on top of this TED, concentrated between protruding intraformational blocks of heterolithics and sandstones

Phase 5

Phase 5 consists of ca. 50 m of interbedded sandstones and mudstones, marked by a gradual decrease in amalgamation of the sandstones and an upward increase of graded sandstone to mudstone (F5; Fig. 5f) and mudstone deposits (F7; Figs. 5H, 9). Neither individual sandstone beds nor small amalgamated packages can be traced continuously across the entire channel belt. As opposed to Phase 4, the normally graded sandstone beds preserve overlying graded mudstone deposits, as well as interbedded mud-dominated thin-bedded sandstone and mudstone intervals between the sand-rich packages (Fig. 10). The exposure of Phase 5 outcrop is less continuous than Phase 4, probably due to increase of mud-dominated intervals (fA5) separating relatively sandier intervals (fA4) of ca. 9 m thick on average. Towards the NE channel margin, the Phase 5 deposits pinch out towards the same ca. 50 – 60-m-thick mass-transport complex (Fig. 13), but less abruptly and more gradually than Phase 4 sandstones. Towards the SW channel margin, the outcrops are not preserved due to the present-day erosional profile (Fig. 4C).

DISCUSSION

Seafloor Topography

Thrust-related seafloor topography in the Magallanes foreland basin, beginning in the Coniacian to Early Campanian (ca. 88 to 74 Ma), produced inversion of structures developed during formation of the Jurassic to Early Cretaceous extensional Rocas Verdes Basin, as is seen in the Malvinas Basin to the south (Fosdick et al. 2011). Sediment routing in the foredeep part of the basin, including the main Cerro Toro axial channel belt (Fig. 3) (Hubbard et al. 2008; Jobe et al. 2010) and the Silla Syncline (Crane and Lowe 2008; Romans et al. 2011; Bernhardt et al. 2011), followed pathways parallel to (and possibly separated by) major compressional structures (Fosdick et al. 2011).

By analogy with control of sediment pathways by variations in shortening in the Monagas Fold–Thrust Belt of Venezuela (Sánchez et al. 2010 *in* Bernhardt et al. 2011), Bernhardt et al. (2011) interpreted the Silla Syncline depocenter as a mini-basin bounded to the east by a high related to a blind thrust progressing eastwards into the basin and to the west by a clastic wedge composed of dominantly fine-grained sediments developed along the topographic front of the thrust.

To maintain topographic control on sedimentation of ca. 1100 m of coarse-grained deposits of the Lago Sofia Member through time, the sedimentation rate must not have exceeded subsidence and structural growth rate (e.g., Smith et al. 2005). A combination of continuous growth of the bounding topographic high, and turbidity current overspill contributing to its relief must have occurred to maintain the system's topographic control (Bernhardt et al. 2011).

The Silla Syncline is thus interpreted to have developed in a piggyback basin behind a topographic high, which separated it from the main basin foredeep drainage system (Crane and Lowe 2008; Bernhardt et al. 2011) (Fig. 14B, C). The clearest evidence in support of the piggyback-basin hypothesis is the onlap of the Paine A sheet system onto a surface that is concordant with the underlying sediments (Fig. 15D), indicating rotation of the substrate above some underlying structure.

Given the complexity of the structures in this thrust-and-fold belt (Fosdick et al. 2011), and the lack of evidence fully supporting any of the interpretations above, discussion on whether the coarse-grained units of the Silla Syncline area represent a fully isolated channel system parallel to (Crane and Lowe 2008; Bernhardt et al. 2011; Bozetti 2017) or tributary to the larger-scale main Cerro Toro system (Jobe et al. 2010; Romans et al. 2011; Malkowski et al. 2015) remains unresolved.

Paleocurrent measurements throughout the Paine C channel system shows that a clear majority, mostly recorded by flutes and clast imbrication in the conglomerates from axis and off-axis areas, and flutes, trough cross-bedding, and ripples in the sandstones, have a mean orientation between 100° and 160° (Fig. 3). Paleocurrent measurements in marginal areas, especially in cross-stratified sandstones, record widely dispersed orientations, which could be related to i) flow expansion and decrease in flow magnitude as channel confinement progressively decreases during infill (Kneller and McCaffrey 1999; Hubbard et al. 2014; Casciano et al. 2019); ii) three-dimensional bedforms such as dune forms, generating inclined surfaces towards a wide range of directions (up to ca. 100° spread) depending on their preservation (Allen 1984); or iii) channel-margin reflection, similar to paleocurrent measurements acquired from ponded systems (Hiscott and Pickering 1984; Haughton 1994; Kneller. 1995; Kneller and McCaffrey 1999; Amy et al. 2000). Channel sinuosity is sometimes invoked to explain the wide spread in paleocurrent directions within the same channel unit (McHargue et al. 2011; Macauley and Hubbard 2013; Casciano et al. 2019). However, measurements from axis and off-axis areas of the Paine C channel system, though recording a slight difference from the proximal parts at the western limb of the Silla Syncline (ca. 100°) to more distal portions at the SE part of the syncline (160°); suggest very low channel sinuosity.

Multi-Phase Depositional Evolution Model

The system's evolution can be divided primarily into four very distinct units: i) an initial widespread mud-dominated deposit, the Laguna Negra Debrite; ii) a conglomeratic unit, consisting of Phases 1 to 3; Figs. 9, 10); iii) the emplacement of the MTC; and iv) a sand-rich unit, Phases 4 and 5 (Figs. 11, 12). The interpreted phases of evolution are illustrated in Figure 14.

Laguna Negra Debrite (LND)

The Paine C channel system has previously been interpreted not to erode substantially into the LND (Crane and Lowe 2008; Bernhardt et al. 2011), in conflict with the evidence documented herein (Fig. 4). The LND is interpreted here as an exceptionally large, mud-dominated transitional event deposit (F7; Fig. 5; Table 1), which erodes into Paine B channel system and surrounding sediments, filling in pre-existing topography, and marking the onset of the Paine C channel system (Fig. 14 – time 1).

Conglomeratic Unit (Paine C1)

The conglomeratic unit (Phases 1, 2, 3; Paine C1 *in* Fig. 2) marks the onset of the channel aggradation. It is ca. 100 m thick in its thickest part, and it is laterally extensive across almost the entire channel belt (Fig. 14). It can be divided into three phases based on facies, facies associations, and degree of channel entrenchment (Fig. 7), as described and interpreted as follows:

Phase 1: Initial Erosion and Channel Entrenchment

The beginning of the conglomeratic unit is marked by incision into the LND on the northwest part of the syncline and Paine A sheets on the southeast part where erosional bypassing flows were generating an initial cut (Fig. 14 - time 2). The end of Phase 1 incision (Figs. 3, 4, 8, 11, 14) is marked by aggradation of the channel belt through deposition of the first phase of Paine C conglomerates, dominated by transitional event deposits (F8; Figs. 6, and 14 - time 3). The deposits vary from channel axis (fA1) through channel off-axis (fA2) and finally channel-margin facies associations (fA3) (Figs. 8, 11, 14). This phase is asymmetric, with a stepped contact at the NE channel margin, interpreted to represent the channel depositional side of a laterally migrating channel system (red rectangle Fig. 3; Log GB40 location *in* Fig. 12); and a northeastward feathering out of the conglomerate deposits firstly into sandstones (F3) subsequently into interbedded sandstone and mudstone (F4) towards the northeast channel margin (Figs. 3, 4, 8).

Phase 2: Intermediate Transitional Phase with Lateral Channel Shifting

Following deposition of the largely aggradational Phase 1 conglomerates, Phase 2 begins with reincision into the Phase 1 (Fig. 14 - time 4) and shows evident facies change documented in a series of sedimentary logs, mainly those at channel-axis and off-axis locations (e.g., Logs GB1 to GB16; GB20, GB21, GB23; Figs. 7, 8, 11, 12, 14). Phase 2 is composed of a mixture between TEDs (F8), clast-supported conglomerates (F1 and F2), bipartite conglomerate and sandstone couplets (F3), and lenticular sandstones (F4; Fig. 5; Table 1), without following any vertical trend (Fig. 7). The deposits in this phase show lateral transition from channel-axis (fA1) to channel-off-axis (fA2) facies associations, but deposits of channel-margin facies association are not apparent. At the NE channel margin, off-axis facies association (fA2) deposits occur adjacent to terrace and/or internal levee facies association (fA6) deposits (Figs. 8, 12), which have previously been described as sediment waves (Campion et al., 2011).

During deposition of the Phase 2 conglomerate, a southwestward shift of the channel axis is recorded, well-preserved in the deposits at the NE channel margin (red rectangle Fig. 3; Figs. 12, 14). This shift is recorded by the southwestward offset of successive erosional surfaces at the northeast channel margin, which are interpreted to contain all the deposits of the aggradational part of the phase 2 (Fig. 12).

<u>Phase 3: Bypass Clast-Supported Conglomerate-Dominated Phase</u>

The last conglomeratic phase is the thickest of all three, ca. 45 m in its thickest part, making up around 50% of the entire Paine C conglomeratic unit in its most axial part (Figs. 8, 10). It records another southwestward shift of the channel axis, mostly observed at the NE channel margin outcrop (red rectangle Fig. 3; Figs. 4, 8). This phase records a significant depositional change in containing mostly facies F1 conglomerates, comprising smaller scour and fill, with very few examples of matrix-rich conglomerates (F2), and conglomerates associated with sandstone (F3), and only subordinate lenticular sandstone beds (F4; Figs. 5, 7, 10; Table 1). The preserved parts of conglomeratic beds are relatively thin and narrow (up to 50 cm thick and ca. 10 to 20 m wide), with erosional base, concave up, highly amalgamated, usually inversely graded or ungraded (Fig. 7). No facies F8 conglomerates

(Fig. 5; Table 1) are recorded in Phase 3. The end of the conglomerate Phase 3 (Fig. 14 - time 7) is marked by a rapid architectural change (see below) (Fig. 14 - time 8).

Sandstone-Dominated Unit (Paine C2)

The sand-rich unit (Paine C2; Figs. 2, 3, 4) marks a major change in the Paine C architecture, from bypass-dominated conglomerates to more aggradational sandstones. The sandstones are confined to the same channel as the Paine C conglomerates, lapping out onto the same thin-bedded succession on the SW channel margin (Figs. 3, 4, 14), and where the margin is visible, onto an MTC towards the northeast (Figs. 13, 14). This 65 – 80-m-thick sandstone-dominated unit is composed mainly of facies associations 4 and 5, and it has been divided into (Figs. 4, 9, 10) a lower, more amalgamated (Fig. 14 - time 8), and an upper non-amalgamated phase separated by a ca. 3-m-thick transitional event deposit recorded across the entire channel belt. The entire sandstone-dominated unit is bounded on the southwest channel margin by laminated carbonate-rich siltstone and claystone interbedded with sparse very fine-grained sandstone, and on the NE channel margin (see Fig. 3 for location) by the mass-transport complex (MTC) (purple deposits *in* Figs. 3, 13), where all deposits thin out rapidly and lap onto the MTC. The outcrops of both the MTC and the channel-bounding mudstones are very limited, and their boundaries are poorly constrained (Figs. 9, 13, 14). The occurrence of MTC-bounding channelized deposits (e.g., Gioia Basin, Gamberi and Rovere 2011; Hansen et al. 2015) resembles transversely emplaced channel-margin MTD topography (e.g., Tek et al. 2020, in the Arro turbidite system) as evidenced by the recognition of a protolith immediately adjacent to the MTDs.

A likely interpretation for the occurrence of an overall thinning- and fining-upwards system of sheetlike sandstones overlying channelized conglomerates is channel backstepping, which occurs due to reduction of flow size with time (Butterworth and Verhaeghe 2012; Morris et al. 2014; Li et al. 2021), shifting depositional loci upstream (Kneller 2003;

Fernandez et al. 2014). Backstepping may happen regardless of changes in sediment supply (Cantelli et al. 2011; Fernandez et al. 2014; Burgess et al. 2019), but its trend is enhanced when deposition is combined with overall waning of the flows (Deptuck et al. 2007; Janocko et al. 2013b; Hodgson et al. 2016; Ferguson et al. 2020; Kneller et al. 2020).

The Paine C system is interpreted as having developed in an active tectonic setting (Fosdick et al. 2011). Similar to other ancient tectonically active sedimentary systems described in the literature (e.g., Arro turbidite system, Arbues et al. 2007a, 2007b; Tek et al. 2020; Gorgoglione Flysch, Casciano et al. 2019), lateral shifting of coarse-grained channel elements, driven either by MTD lateral confinement (Tek et al. 2020) or simply structural growth (Casciano et al. 2019), is interpreted as diversion due to synsedimentary tectonics.

Aggradational Versus Bypass-Dominated Channel Systems

Conglomeratic facies recognized in submarine gravelly channels provide valuable information about transport and depositional processes. Facies composed of low-matrix-content clast-supported conglomerates (F1), with subordinate high-matrix-content clast-supported conglomerates, associated or not with lenticular sandstones (F2 and F3 respectively), are interpreted to occur in systems dominated by high-energy currents, where gravel moves largely as bedload, generating large-scale traction structures (Winn and Dott 1977; Piper et al. 1985; Piper and Kontopoulos 1994; Wynn et al. 2002), and most of the sand and finer sediment load bypasses (e.g., Stevenson et al. 2015), largely in suspension.
The distinctive clast- to matrix-supported conglomerates in this system (here termed transitional event deposits, TEDs, F8; Bozetti et al. 2018) have been described in differing degrees of detail by Scott (1966), Winn and Dott (1979), Sohn (2000), Beauboeuf (2004), Crane and Lowe (2008), Hubbard et al. (2008), Bernhardt et al. (2011), Romans et al. (2011) and Bozetti et al. (2018). However, there is overall consistency in the descriptions of the lithofacies, the salient features of which are: a basal surface that often has very large-scale

flute casts (e.g., Winn and Dott 1979; Sohn et al. 2000, Beauboeuf 2004); succeeded by an inversely to normally graded, often imbricated clast-supported interval (Winn and Dott 1979; Sohn et al. 2000); this is transitional upwards, with decreasing clast abundance, into a matrix-supported interval of sandy mudstone, in which both the matrix and clasts are often normally graded (Crane 2004). These have also been described as slurry flows by Crane and Lowe (2008) and Hubbard et al. (2008), but the characteristics of TEDs are considerably at odds with those of slurry beds as described by Lowe and Guy (2000), where the term was first employed to describe somewhat similar matrix-rich sandstones.

There has been a range of interpretations of the process(es) responsible for their deposition. Winn and Dott (1979) suggested three possible alternative mechanisms (reprised by Hubbard et al. 2008): (a) the settling of large clasts through a debris flow to form a traction-dominated bedload; (b) the progressive entrainment of mud into initially turbulent flows (responsible for the basal erosion and traction-dominated basal layer) to transform into flows with more cohesive strength, as in models for the origin of so-called hybrid beds (e.g., Haughton et al. 2009; Kane and Pontén 2012); (c) generation of turbidity currents from parental debris flows (cf. Hampton 1972) by surface or body transformation (e.g., Felix and Peakall 2006) or detachment of the head of hydroplaning debris flows (Sohn et al. 2000).

There is general consensus that the upper parts of the beds can be interpreted as the product of debris flows, in which gravel is largely suspended by the matrix (non-Newtonian flow; e.g., Crowell 1957; Scott 1966; Stanley 1974; Embley 1976; Haughton et al. 2009; Kane and Pontén 2012; Bozetti et al. 2018). Winn and Dott (1979) rejected the hypothesis that the larger, heavier clasts have sunk through the matrix to the base of the flow to form the basal clast-supported layer behaving as a kind of traction carpet or shear layer beneath an overriding debris flow, on the grounds that the basal flute casts must have been produced by turbulent flow (see also Sohn 2000). Winn and Dott (1979) and Sohn et al. (2002) considered the clast-supported layer to have been driven by an overriding turbulent suspension. If so, the transition from a turbulent dispersed suspension to a denser, more cohesive and perhaps laminar dispersion must have been transitional, given the progressive upwards change from clast support to matrix support. Unlike the deposits generated by high-energy bypassing flows, where gravel moves dominantly as bedload and the preserved remnant of the deposit is typically narrow and thin (e.g., facies F1, 0.5 to 1 m thick and 20 to 50 m wide), TEDs are preserved as beds ca. 3 to 30 m thick that may be laterally persistent over kilometers (e.g., Crane and Lowe 2008). In such flows, sediment bypass is probably minimal, perhaps with only very fine-grained sediment bypassing through the channel as a remnant low-density turbulent cloud at the latest stage of flow evolution (Bozetti et al. 2018).

Differences in processes that dominate channel systems are reflected in major differences in their architecture. Channel systems dominated by high-energy turbulent processes move gravel as bedload and bypass large amounts of suspended sediment load (e.g., Stromboli slope valley, Gamberi and Marani 2011; Rosario Formation, Kneller et al. 2020). In many systems, evolution from initially erosive (degradation) to aggradation may repeat multiple times at a range of scales until the channel system ceases to be active, but often with fining-upwards sequences at a range of scales, including that of the system as a whole (e.g., Sprague et al. 2002; Mayall et al. 2006; Kneller et al. 2020). The mechanism that guides this multiphase evolution is interpreted to be related mostly to change in the equilibrium profile, driven by changes in flow properties (Kneller 2003) or changes in base level due to erosion or syndepositional tectonics (Pirmez et al. 2000). In most published cases the architecture of the aggradational phase is dominated by deposition largely from flows that are inferred to be broadly similar to those that dominate during the bypass phase, i.e., turbulent gravity-driven suspensions, perhaps with some bedload transport, but with a significant amount of suspended sediment fallout.

By contrast, in Phase 1 of the Paine C system, laterally persistent and highly depositional TEDs are the most abundant facies. This leads to the conclusion that the fill stage of Phase 1 was largely aggradational, possibly involving significant adjustment to the equilibrium profile. Phase 2 is likewise dominated by TEDs, though to a lesser extent than Phase 1. Phase 3 consists almost entirely of clast-supported (bypass-related) conglomerates except in the adjacent terrace and/or internal levee, suggesting a system dominated by bedload transport beneath powerful currents, carrying sandy suspended load through the system, with a more gradual aggradation. Phases 4 and 5 represent an overall waning and perhaps backstepping of the system, dominated by deposition from suspension fallout of sand, with only sporadic deposition of TEDs.

This study reveals a somewhat different architecture from that characterized by (a) erosion and complete sediment bypass to (b) aggradation of bedload-dominated channel fills with significant bypass of suspended load, which is an architecture that has been recognized in (or at least a model that has been applied to) a number of slope channel systems (Sullivan et al. 2000; Sprague et al. 2002; Abreu et al. 2003; Posamentier 2003; Mayall et al. 2006; McHargue et al. 2011; Hubbard et al. 2012; Fildani et al. 2013; Li et al. 2018; Kneller et al. 2020). The Paine C channel system (and likely the entire main channel belt represented by the Lago Sofia Member of the Cerro Toro Fm., e.g., Winn and Dott 1979; Hubbard et al. 2008; Jobe et al. 2010), based on the common occurrence of the conglomeratic facies described here as transitional event deposits (F8), illustrates an architecture that has not previously been described in detail, made possible only by the exceptional exposure resulting from the fire of 2011. Systems that do not benefit from the same level of outcrop, or those in the subsurface, may have been erroneously interpreted according to an inappropriate submarine-channel model, underestimating the distinction between bypass-dominated channel systems (e.g., Kneller et al. 2020) and debrite-rich and more aggradational systems similar to the Cerro Toro Fm. (e.g., Austrian Molasse Basin, Hubbard et al. 2009; Bernhardt et al. 2012; see details in Bozetti et al. 2018).

CONCLUSIONS

The main conclusions of the Paine C channel system are summarized as follows: Based on the detailed architectural analysis of the Paine C, combined with examples from the literature, two types of submarine channel systems can be differentiated based on facies and architecture, generating highly distinct end members, especially from a reservoir perspective. Bypass-dominated systems are composed dominantly of deposits from flows moving gravel as bedload, bypassing most of their sediment load in suspension, generating mud-poor sand- or gravel-prone deposits, and therefore good reservoir prospects, downdip from the channel as well as within it. By contrast, aggradational systems are dominantly composed of deposits that are the product of transitional flows, in which most of the sediment from the parent flow is deposited in a highly mixed, matrix-supported deposit, with very poor fluid-reservoir properties, probably with only minor amounts of (dominantly fine-grained) sediment bypass from the residual low-density turbulent cloud, and thus lower probability of downdip sand accumulations.

Recognizing the differences between bypass-dominated and aggradation-dominated channel systems has major potential significance from a fluid-reservoir perspective. Bypass-dominated systems will tend to consist of highly porous and permeable lithologies that are well-connected both laterally and vertically. By contrast, systems such as Paine C, where the aggradation is largely via deposition of mud-rich and laterally-persistent deposits, will not only have reduced reservoir volumes but possess significantly reduced vertical connectivity. These distinctions would be critical to flow modelling (e.g., Mendez 2022).

ACKNOWLEDGMENTS

The Brazilian National Council for Scientific and Technological Development (CNPq), BG Brazil (now Shell) and Agência Nacional do Petróleo (ANP) are thanked for their support of the Ph.D. project of Bozetti. The PRACCS research consortium at Aberdeen, supported by Dong Energy, BP, PetroChina, RWE-Dea, Tullow Oil, DetNorsk (AkerBP), BG (Shell), and Statoil (Equinor), funded the fieldwork for co-authors in Chile at various stages. This work was also in part supported by the National Science Foundation of China (NSFC, Grant 41720104001). We also thank the various Ph.D. students and postdoctoral researchers who accompanied us from 2012 to 2017, in particular Dugmar Isabel Mendez, Viki Valdez, Qun Liu, and Jianan Wu. We thank as well the University of Strasbourg's *IdEx Attactivité 1er equipment ou 1ères actions de recherche* for funding the continuation of this study through QRADS (quantifying reservoir architecture in deep-water systems). Last but not least we thank the extremely valuable comments by the Andrea Fildani, Zane Jobe, and an anonymous reviewer.

REFERENCES

Abreu, V., Sullivan, M., Pirmez, C., and Mohrig, D., 2003, Lateral accretion packages (LAPs): an important reservoir element in deep water sinuous channels: Marine and Petroleum Geology, v. 20, no. 6-8, p. 631-648.

Allen, J.R.L., 1982, Sedimentary Structures: Their Character and Physical Basis. Elsevier, Amsterdam, Developments in Sedimentology 30A, 593 p.

Allen, J.R.L., 1984, Sedimentary Structures: Their Character and Physical Basis: Amsterdam, Elsevier, Developments in Sedimentology 30, 663 p.

Amy, L.A., Kneller, B., and McCaffrey, W.D., 2000, Evaluating the links between turbidite characteristics and gross system architecture: upscaling insights from the turbidite sheet-system of Peïra Cava, SE France: Deep Water Reservoirs of the World, p. 1-15.

Arbués, P., Mellere, D., Falivene, O., Fernández, O., Muñoz, J.A., Marzo, M., and de Gibert, J.M., 2007a, Context and architecture of the Ainsa-1- quarry channel complex, Spain, *in* Nilsen, T.H., Shew, R.D., Steffens, G.S. and Studlick, J.R.J., (eds.), Atlas of Deep-Water Outcrops: American Association of Petroleum Geologists, Studies in Geology 56, p. 20.

Arbués, P., Mellere, D., Puig, M. and Marzo, M., 2007b, The effect of slumping on sandstone distribution in the Arro turbidites, Los Molinos Road, Spain, *in* Nilsen, T.H., Shew, R.D., Steffens, G.S., and Studlick, J.R.J., (eds.), Atlas of Deep-Water Outcrops: American Association of Petroleum Geologists, Studies in Geology 56, p. 333-335.

Armitage, D.A., Romans, B.W., Covault, J.A., and Graham, S.A., 2009, The influence of mass-transport-deposit surface topography on the evolution of turbidite architecture: The Sierra Contreras, Tres Pasos Formation (Cretaceous), southern Chile: Journal of Sedimentary Research, v. 79, no. 5, p. 287-301.

Barton, M.D., Craig, P., Prather, B.E., Copus, J., 2007a, Facies architecture of channel–levee deposits, Lago Nordenskjold and Laguna Melizzas Sur, Cerro Toro formation, Chile, *in* Nilsen, H., Shew, R.D., Steffens, G.S., and Studlick, J., (eds.), Deepwater Outcrops of the World Atlas: Amercan Association of Petroleum Geologists, Studies in Geology 56, p. 157e161. Barton, M.D., Steffens, G.S. and O'Byrne, C.J., 2007. Facies architecture of a submarine-slope channel complex, Condor West channel, Cerro Toro Formation, Chile, p. 149-153.

Beaubouef, R.T., 2004, Deep-water leveed-channel complexes of the Cerro Toro Formation, Upper Cretaceous, southern Chile: American Association of Petroleum Geologists, Bulletin, v. 88, p. 1471-1500.

Bernhardt, A., Jobe, Z.R., and Lowe, D.R., 2011, Stratigraphic evolution of a submarine channel-lobe complex system in a narrow fairway within the Magallanes foreland basin, Cerro Toro Formation, southern Chile: Marine and Petroleum Geology, v. 28, p. 785-806.

Bernhardt, A., Jobe, Z.R., Grove, M., and Lowe, D.R., 2012. Palaeogeography and diachronous infill of an ancient deep-marine foreland basin, Upper Cretaceous Cerro Toro Formation, Magallanes Basin: Basin Research, v. 24(3), p. 269-294.

Biddle, K.T., Uliana, M.A., Mitchum Jr, R.M., Fitzgerald, M.G., and Wright, R.C., 1986, The stratigraphic and structural evolution of the central and eastern Magallanes Basin, southern South America: Foreland Basins, p. 41-61.

Bozetti, G., 2017, Stratigraphy and architecture of a coarse-grained deep-water system within the Cretaceous Cerro Toto formation, Silla Syncline area, southern Chile [PhD Thesis]: University of Aberdeen, Aberdeen, U.K., 385 p.

Bozetti, G., Cronin, B.T., Kneller, B.C., and Jones, M.A., 2018, Chapter Five: Deep-Water Conglomeratic Megabeds: Analogues for Event Beds of the Brae Formation of the South Viking Graben, North Sea, *in* Turner, C.C., and Cronin, B.T., (eds.), Rift-related coarse-grained submarine fan reservoirs; the Brae Play, South Viking Graben, North Sea: American Association of Petroleum Geologists, Memoir 115, p. 119-153.

Brunt, R.L., Hodgson, D.M., Flint, S.S., Pringle, J.K., Di Celma, C., Prélat, A., and Grecula, M., 2013, Confined to unconfined: anatomy of a base of slope succession, Karoo Basin, South Africa: Marine and Petroleum Geology, v. 41, p. 206-221.

Burgess, P.M., Masiero, I., Toby, S.C., and Duller, R.A., 2019, A big fan of signals? Exploring autogenic and allogenic process and product in a numerical stratigraphic forward model of submarine-fan development: Journal of Sedimentary Research, v. 89, no. 1, p. 1-12.

Butterworth, P.J., and Verhaeghe, J., 2012, Evolution of a Pliocene upper slope channel complex set, Giza Field, West Nile Delta, Egypt: interaction of sedimentation and tectonics, *in* Rosen, N.C., Weimer, P., Coutes dos Anjos, S.M., Henrickson, S., Marques, E., Mayall, M., and Schroeder, F., (eds.), New Understanding of Petroleum Systems on

Continental Margins of the World: SEPM (Society for Sedimentary Geology), Gulf Coast Section, 32nd Annual Bob F. Perkins Research Conference, Proceedings, p. 541-572.

Calderon, M., Fildani, A., Herve, F., Fanning, C.M., Weislogel, A., Cordani, U., 2007, Late Jurassic bimodal magmatism in the northern seafloor remnant of the Rocas Verdes basin, southern Patagonian Andes. Journal of the Geological Society, v. 164, p. 1011-1022.

Callow, R.H., Kneller, B., Dykstra, M., and McIlroy, D., 2014, Physical, biological, geochemical and sedimentological controls on the ichnology of submarine canyon and slope channel systems: Marine and Petroleum Geology, v. 54, p. 144-166.

Camacho, H., Busby, C.J., and Kneller, B., 2002, A new depositional model for the classical turbidite locality at San Clemente State Beach, California: American Association of Petroleum Geologists, Bulletin, v. 86, p. 1543-1560.

Campion, K.M., Sprague, A.R., Mohrig, D., Lovell, R.W., Drzewiecki, P.A., Sullivan, M.D., Ardill, J.A., Jensen, G.N., and Sickafoose, D.K., 2000, Outcrop expression of confined channel complexes, *in* Weimer, P., Slatt, R.M., Coleman, J., Rosen, N.C., Nelson, H., Bouma, A.H., Styzen, M.J., and Lawrence, D.T., (eds.), Deep-Water Reservoirs of the World: SEPM (Society for Sedimentary Geology), Gulf Coast Section, p. 127-151.

Campion, K.M., 2005, Architecture and lithofacies of the Capistrano Formation (Miocene-Pliocene), San Clemente, California: v. 100, SEPM (Society for Sedimentary Geology), Pacific Section, 84p.

Campion, K.M., Dixon, B.T., Scott, E.D., 2011, Sediment Waves and Depositional Implications for Fine-Grained Rocks in the Cerro Toro Formation (Upper Cretaceous), Silla Syncline, Chile: Marine and Petroleum Geology, v. 28, p. 761-784.

Cantelli, A., Pirmez, C., Johnson, S., and Parker, G., 2011, Morphodynamic and stratigraphic evolution of self-channelized subaqueous fans emplaced by turbidity currents: Journal of Sedimentary Research, v. 81, no. 3, p. 233-247.

Casciano, C.I., Patacci, M., Longhitano, S.G., Tropeano, M., McCaffrey, W.D., and Di Celma, C., 2019, Multi-scale analysis of a migrating submarine channel system in a tectonically-confined basin: The Miocene Gorgoglione Flysch Formation, southern Italy: Sedimentology, v. 66, no. 1, p. 205-240.

Cecioni, G.O., 1957, Cretaceous flysch and molasse in Departmento Ultima Esperanza, Magellanes Province, CUle: American Association of Petroleum Geologists, Bulletin, v. 41, p. 538-564.

Coleman, J.L., 2000, Reassessment of the Cerro Toro (Chile) sandstones in view of channel-levee–overbank reservoir continuity issues, *in* Weimer, P., Slatt, R.M., Coleman, J.L., Rosen, N.C., Nelson, H., Bouma, A.H., Styzen M.J., and Lawrence D.T., (eds.), Deep-Water Reservoirs of the World: SEPM (Society for Sedimentary Geology), Gulf Coast Section, 20th Annual Conference, p. 252-262

Collinson, J.D., and Thompson, D.B., 1982, Sedimentary Structures: George Allen and Unwin, London, 194 p.

Crane, W.H., 2004, Depositional history of the Upper Cretaceous Cerro Toro Formation, Silla syncline, Magallanes basin, Chile: Ph.D. thesis, Stanford University, Stanford, California, 275 p.

Crane, W.H., and Lowe, D.R., 2008, Architecture and evolution of the Paine channel complex, Cerro Toro formation (Upper Cretaceous), Silla syncline, Magallanes basin, Chile: Sedimentology, v. 55, no. 4, p. 979-1009.

Crane, W.H., and Lowe, D.R., 2009, Outcrop 5. NW Margin of the Paine 'C' Channel Complex, Silla Syncline, *in* Fildani, A., Hubbard, S.M., and Romans, B.W., (eds.), Outcrop Atlas and Field Guide For SEPM Research Conference, February 22–28, 2009, p. 29-30.

Cronin, B.T., Akhmetzhanov, A.M., Mazzini, A., Akhmanov, G., Ivanov, M., and Kenyon, N.H., 2005, Morphology, evolution and fill: implications for sand and mud distribution in filling deep-water canyons and slope channel complexes: Sedimentary Geology, v. 179, no. 1-2, p. 71-97.

Crowell, J.C., 1957, Origin of pebbly mudstones: Geological Society of America, Bulletin, v. 68, no. 8, p. 993-1010.

Dalziel, I.W., de Wit, M.J., and Palmer, K.F., 1974, Fossil marginal basin in the southern Andes: Nature, v. 250, no. 5464, p. 291-294.

Daniels, B.G., Hubbard, S.M., Romans, B.W., Malkowski, M.A., Matthews, W.A., Bernhardt, A., Kaempfe, S.A., Jobe, Z.R., Fosdick, J.C., Schwartz, T.M., and Fildani, A., 2019, Revised chronostratigraphic framework for the Cretaceous Magallanes–Austral Basin, Ultima Esperanza Province, Chile: Journal of South American Earth Sciences, v. 94, no. 102209.

Deptuck, M.E., Sylvester, Z., Pirmez, C., and O'Byrne, C., 2007, Migration-aggradation history and 3-D seismic geomorphology of submarine channels in the Pleistocene Benin–Major Canyon, western Niger Delta slope: Marine and Petroleum Geology, v. 24, p. 406-433.

Devries, M.B., and Lindholm, R.M., 1994, Internal architecture of a channel-levee complex, Cerro Toro Formation, southern Chile, southern Chile, *in* Submarine Fans and Turbidite Systems: Sequence Stratigraphy, Reservoir Architecture and Production Characteristics (Weimer, P., Bouma, A.H., and Perkins, B.F.), SEPM (Society for Sedimentary Geology) Gulf Coast Section, 15th Annual Conference, p. 105-114.

De Wit, M.J., and Stern, C.R., 1981, Variations in the degree of crustal extension during formation of a back-arc basin: Tectonophysics, v. 72, no. 3-4, p. 229-260.

Di Celma, C.N., Brunt, R.L., Hodgson, D.M., Flint, S.S., and Kavanagh, J.P., 2011, Spatial and temporal evolution of a Permian submarine slope channel-levee system, Karoo Basin, South Africa: Journal of Sedimentary Research, v. 81, no. 8, p. 579-599.

Embley, R.W., 1976, New evidence for occurrence of debris flow deposits in the deep sea: Geology, v. 4, no. 6, p. 371-374.

Felix, M., and Peakall, J., 2006, Transformation of debris flows into turbidity currents: mechanisms inferred from laboratory experiments: Sedimentology, v. 53, no. 1, p. 107-123.

Ferguson, R.A., Kane, I.A., Eggenhuisen, J.T., Pohl, F., Tilston, M., Spychala, Y.T., and Brunt, R.L., 2020, Entangled external and internal controls on submarine fan evolution: an experimental perspective: The Depositional Record, v. 6, no. 3, p. 605-624.

Fernandez, R.L., Cantelli, A., Pirmez, C., Sequeiros, O., and Parker, G., 2014, Growth patterns of subaqueous depositional channel lobe systems developed over a basement with a downdip break in slope: laboratory experiments: Journal of Sedimentary Research, v. 84, p. 168-182.

Fildani, A., Cope, T.D., Graham, S.A., and Wooden, J.L., 2003, Initiation of the Magallanes foreland basin: Timing of the southernmost Patagonian Andes orogeny revised by detrital zircon provenance analysis: Geology, v. 31, no. 12, p. 1081-1084.

Fildani, A., and Hessler, A.M., 2005, Stratigraphic record across a retroarc basin inversion: Rocas Verdes-Magallanes basin, Patagonian Andes, Chile: Geological Society of America, Bulletin, v. 117, no. 11-12, p. 1596-1614.

Fildani, A., Hubbard, S.M., and Romans, B.W., 2009, Stratigraphic evolution of deep-water architecture: Examples of controls and depositional styles from the Magallanes Basin, southern Chile, with contribution from: Covault, J.A., Crane, W.H., Bernhardt, A., Jobe, Z.R., Armitage, D.A., Fosdick, J.C., Shultz, M.R, and Clark, J., (eds.), SEPM (Society for Sedimentary Geology) field guide, no. 10, 73p.

Fildani, A., Hubbard, S.M., Covault, J.A., Maier, K.L., Romans, B.W., Traer, M., and Rowland, J.C., 2013, Erosion at inception of deep-sea channels: Marine and Petroleum Geology, v. 41, p. 48-61.

Fosdick, J.C., Romans, B.W., Fildani, A., Bernhardt, A., Calderón, M., and Graham, S.A., 2011, Kinematic evolution of the Patagonian retroarc fold-and-thrust belt and Magallanes foreland basin, Chile and Argentina, 51 30' S: The Geological Society of America, Bulletin, v. 123, no. 9-10, p. 1679-1698.

Gamberi, F., and Marani, M., 2011, Geomorphology and sedimentary processes of a modern confined braided submarine channel belt (Stromboli Slope Valley, southeastern Tyrrhenian Sea): Journal of Sedimentary Research, v. 81, p. 686-701.

Gamberi, F., and Rovere, M., 2011, Architecture of a modern transient slope fan (Villafranca fan, Gioia basin-Southeastern Tyrrhenian Sea): Sedimentary Geology, v. 236, no. 3-4, p. 211-225.

Gamberi, F., Rovere, M., Dykstra, M., Kane, I.A., and Kneller, B.C., 2013, Integrating modern seafloor and outcrop data in the analysis of slope channel architecture and fill: Marine and Petroleum Geology, v. 41, p. 83-103.

Ghiglione, M.C., Likerman, J., Barberón, V., Giambiagi, L.B., Aguirre-Urreta, B., and Suarez, F., 2014, Geodynamic context for the deposition of coarse-rained deep-water axial channel systems in the Patagonian Andes: Basin Research, v. 26, no. 6, p. 726-745.

Gonzales, J., and Aydin, A., 2008, Structural characterization of deep-water deposits in a foreland basin, Silla Syncline (Chilean Patagonia), with applications to depositional processes: Journal of Structural Geology, v. 30, no. 9, p. 1095-1108.

Grecula, M., Flint, S.S., Wickens, H.D.V., and Johnson, S.D., 2003, Upward-thickening patterns and lateral continuity of Permian sand-rich turbidite channel fills, Laingsburg Karoo, South Africa: Sedimentology, v. 50, no. 5, p. 831-853.

Hampton, M.A., 1972, The role of subaqueous debris flow in generating turbidity currents: Journal of Sedimentary Petrology, v. 42, no. 4, p. 775-793.

Hansen, L.A., Callow, R.H., Kane, I.A., Gamberi, F., Rovere, M., Cronin, B.T., and Kneller, B.C., 2015, Genesis and character of thin-bedded turbidites associated with submarine channels: Marine and Petroleum Geology, v. 67, p. 852-879.

Hansen, L., Callow, R., Kane, I., and Kneller, B., 2017a, Differentiating submarine channel related thin-bedded turbidite facies: outcrop example from the Rosario Formation, Mexico: Sedimentary Geology, v. 358, p. 19-34.

Haughton, P.D., 1994, Deposits of deflected and ponded turbidity currents, Sorbas Basin, Southeast Spain: Journal of sedimentary Research, v. 64, no. 2, p. 233–246.

Haughton, P., Davis, C., McCaffrey, W., and Barker, S., 2009, Hybrid sediment gravity flow deposits-classification, origin and significance: Marine and Petroleum Geology, v. 26, no. 10, p. 1900-1918.

Hay, A.E., 1987, Turbidity currents and submarine channel formation in Rupert Inlet, British Columbia: 2. The roles of continuous and surge-type flow: Journal of Geophysical Research: Oceans, v. 92, no. C3, p. 2883-2900.

Hiscott, R.N., and Pickering, K.T., 1984, Reflected turbidity currents on an Ordovician basin floor, Canadian Appalachians: Nature, v. 311, no. 5982, p. 143-145.

Hodgson, D.M., Kane, I.A., Flint, S.S., Brunt, R.L., and Ortiz-Karpf, A., 2016, Time-transgressive confinement on the slope and the progradation of basin-floor fans: Implications for the sequence stratigraphy of deep-water deposits: Journal of Sedimentary Research, v. 86, no.1, p. 73-86.

Hubbard, S.M., Romans, B.W., and Graham, S.A., 2008, Deep-water foreland basin deposits of the Cerro Toro Formation, Magallanes basin, Chile: architectural elements of a sinuous basin axial channel belt: Sedimentology, v. 55, no. 5, p. 1333-1359.

Hubbard, S.M., and Schultz, M.R., 2008, Deep burrows in submarine fan-channel deposits of the Cerro Toro Formation (Cretaceous), Chilean Patagonia: implications for firm ground development and colonization in the deep sea: Palaios, v. 23, p. 223-232.

Hubbard, S.M., de Ruig, M.J., and Graham, S.A., 2009, Confined channel–levee complex development in an elongate depo-center: deep-water Tertiary strata of the Austrian Molasse basin: Marine and Petroleum Geology, v. 26, no. 1, p. 85-112.

Hubbard, S.M., Fildani, A., Romans, B.W., Covault, J.A., and McHargue, T.R., 2010, High-relief slope clinoform development: Insights from outcrop, Magallanes Basin, Chile: Journal of Sedimentary Research, v. 80, no. 5, p .357-375.

Hubbard, S.M., Maceachern, J.A. and Bann, K.L., 2012, Slopes: Elsevier, Developments in Sedimentology, v. 64, p. 607-642.

Hubbard, S.M., Covault, J.A., Fildani, A., and Romans, B.W., 2014, Sediment transfer and deposition in slope channels: deciphering the record of enigmatic deep-sea processes from outcrop: Geological Society of America, Bulletin, v. 126, p. 857-871.

Hubbard, S.M., Jobe, Z.R., Romans, B.W., Covault, J.A., Sylvester, Z., and Fildani, A., 2020, The stratigraphic evolution of a submarine channel: Linking seafloor dynamics to depositional products: Journal of Sedimentary Research, v. 90, no. 7, p. 673-686.

Janocko, M., Nemec, W., Henriksen, S., and Warchoł, M., 2013b, The diversity of deepwater sinuous channel belts and slope valley-fill complexes: Marine and Petroleum Geology, v. 41, p. 7-34.

Jobe, Z.R., Bernhardt, A., and Lowe, D.R., 2010, Facies and architectural asymmetry in a conglomerate-rich submarine channel fill, Cerro Toro Formation, Sierra del Toro, Magallanes Basin, Chile: Journal of Sedimentary Research, v. 80, no. 12, p. 1085-1108.

Kane, I.A., Kneller, B.C., Dykstra, M., Kassem, A., and McCaffrey, W.D., 2007, Anatomy of a submarine channel–levee: an example from Upper Cretaceous slope sediments, Rosario Formation, Baja California, Mexico: Marine and Petroleum Geology, v. 24, p. 540-563.

Kane, I.A., McCaffrey, W.D., Peakall, J., and Kneller, B.C., 2010 Submarine channel levee shape and sediment waves from physical experiments: Sedimentary Geology, v. 223, no. 1-2, p. 75-85.

Kane, I.A., and Hodgson, D.M., 2011, Sedimentological criteria to differentiate submarine channel levee subenvironments: exhumed examples from the Rosario Fm. (Upper Cretaceous) of Baja California, Mexico, and the Fort Brown Fm. (Permian), Karoo basin, S. Africa: Marine and Petroleum Geology, v. 28, no. 3, p. 807-823.

Kane, I.A., and Pontén, A.S., 2012, Submarine transitional flow deposits in the Paleogene Gulf of Mexico: Geology, v. 40, no. 12, p. 1119-1122.

Katz, H.R., 1963, Revision of Cretaceous stratigraphy in Patagonian Cordillera of Ultima Esperanza, Magallanes Province, Chile: American Association of Petroleum Geologists Bulletin, v. 47, no. 3, p. 506-524.

Kneller, B., 1995, Beyond the turbidite paradigm: physical models for deposition of turbidites and their implications for reservoir prediction, *in* Hartley, A.J., and Prosser, D.J., (eds.), Geological Society of London, Special Publications, no. 94, p. 31-49.

Kneller, B., 2003, The influence of flow parameters on turbidite slope channel architecture: Marine and Petroleum Geology, v. 20, no. 6-8, p. 901-910.

Kneller, B.C., and Branney, M.J., 1995, Sustained high-density turbidity currents and the deposition of thick massive sands: Sedimentology, v. 42, no. 4, p. 607-616.

Kneller, B., and Buckee, C., 2000, The structure and fluid mechanics of turbidity currents: a review of some recent studies and their geological implications: Sedimentology, v. 47, p. 62-94.

Kneller, B., and McCaffrey, W., 1999, Depositional effects of flow nonuniformity and stratification within turbidity currents approaching a bounding slope; deflection, reflection, and facies variation: Journal of Sedimentary Research, v. 69, no. 5, p. 980-991.

Kneller, B., Edwards, D., McCaffrey, W., and Moore, R., 1991, Oblique reflection of turbidity currents: Geology, v. 19, no. 3, p. 250-252.

Kneller, B., Bozetti, G., Callow, R., Dykstra, M., Hansen, L., Kane, I., Li, P., McArthur, A., Catharina, A.S., dos Santos, T., and Thompson, P., 2020, Architecture, process, and environmental diversity in a late Cretaceous slope channel system: Journal of Sedimentary Research, v. 90, no. 1, p. 1-26.

Li, P., Kneller, B.C., Hansen, L., and Kane, I.A., 2016, The classical turbidite outcrop at San Clemente, California revisited: An example of sandy submarine channels with asymmetric facies architecture: Sedimentary Geology, v. 346, p. 1-16.

Li, P., Kneller, B., Thompson P., Bozetti, G., and Santos, T.D., 2018, Architectural and facies organisation of slope channel fills: Upper Cretaceous Rosario Formation, Baja California, Mexico: Marine and Petroleum Geology, v. 92, p. 632-649.

Li, P., Kneller, B., and Hansen, L., 2021, Anatomy of a gas-bearing submarine channel–lobe system on a topographically complex slope (offshore Nile Delta, Egypt): Marine Geology, v. 437, p. 106496.

Lowe, D.R., 1975, Water escape structures in coarse-grained sediments: Sedimentology, v. 22, no. 2, p. 157-204.

Lowe, D.R., 1982, Sediment gravity flows II, Depositional models with special reference to the deposits of high-density turbidity currents: Journal of Sedimentary Petrology, v. 52, no. 1, p. 279-297.

Lowe, D.R., and Guy, M., 2000, Slurry-flow deposits in the Britannia Formation (Lower Cretaceous), North Sea: A new perspective on the turbidity current and debris flow problem: Sedimentology, v. 47, p. 31–70

Macauley, R.V., and Hubbard, S.M., 2013, Slope channel sedimentary processes and stratigraphic stacking, Cretaceous Tres Pasos Formation slope system, Chilean Patagonia: Marine and Petroleum Geology, v. 41, p. 146-162.

Macellari, C.E., Barrio, C.A., and Manassero, M.J., 1989, Upper Cretaceous to Paleocene depositional sequences and sandstone petrography of southwestern Patagonia (Argentina and Chile): Journal of South American Earth Sciences, v. 2, no. 3, p. 223-239.

Maier, K.L., Gales, J.A., Paull, C.K., Rosenberger, K., Talling, P.J., Simmons, S.M., Gwiazda, R., McGann, M., Cartigny, M.J., Lundsten, E., and Anderson, K., 2019, Linking direct measurements of turbidity currents to submarine canyon-floor deposits: Frontiers in Earth Science, v. 7, 144 p.

Malkowski, M.A., Sharman, G.R., Graham, S.A., and Fildani, A., 2015, Characterisation and diachronous initiation of coarse clastic deposition in the Magallanes-Austral foreland basin, Patagonian Andes: Basin Research, v. 29, p. 298-326.

Malkowski, M.A., Jobe, Z.R., Sharman, G.R., and Graham, S.A., 2018, Down-slope facies variability within deep-water channel systems: Insights from the Upper Cretaceous Cerro Toro Formation, southern Patagonia: Sedimentology, v. 65, no. 6, p. 1918-1946.

Mayall, M., Jones, E., and Casey, M., 2006, Turbidite channel reservoirs–Key elements in facies prediction and effective development: Marine and Petroleum Geology, v. 23, no. 8, p. 821-841.

Mayall, M., and Kneller, B., 2021, Seismic interpretation workflows for deep-water systems: A practical guide for the subsurface: American Association of Petroleum Geologists, Bulletin, v. 105, no. 11, p. 2127-2157.

McCaffrey, W., and Kneller, B., 2001, Process controls on the development of stratigraphic trap potential on the margins of confined turbidite systems and aids to reservoir evaluation: American Association of Petroleum Geologists, Bulletin, v. 85, no. 6, p. 971-988.

McHargue, T., Pyrcz, M.J., Sullivan, M.D., Clark, J.D., Fildani, A., Romans, B.W., Covault, J.A., Levy, M., Posamentier, H.W., and Drinkwater, N.J., 2011, Architecture of turbidite channel systems on the continental slope: patterns and predictions: Marine and Petroleum Geology, v. 28, p. 728-743.

Mendez, D.I., 2022, 3D Simulation of Heterogeneities in Conglomeratic Slope Channel Architectures [PhD Thesis]: University of Aberdeen, Aberdeen, U.K., 312 p.

Morris, W.R., and Normark, W.R., 2000, Sedimentologic and geometric criteria for comparing modern and ancient sandy turbidite elements, *in* Weimer, P., (ed.), Deep-Water Reservoirs of the World: 20th Annual Research Conference, Golf Coast Section, SEPM (Society for Sedimentary Geology), p. 606-628,

Morris, E., Hodgson, D., Brunt, R., and Flint, S., 2014, Origin, evolution and anatomy of silt-prone submarine external levees: Sedimentology v. 61, p. 1734-1763.

Morris, E.A., Hodgson, D.M., Flint, S., Brunt, R.L., Luthi, S.M., and Kolenberg, Y., 2016, Integrating outcrop and subsurface data to assess the temporal evolution of a submarine channel–levee system: American Association of Petroleum Geologists, Bulletin, v. 100, no. 11, p. 1663-1691.

Mulder, T., and Alexander, J., 2001, The physical character of subaqueous sedimentary density flows and their deposits: Sedimentology, 48, no. 2, p. 269-299.

Mutti, E., 1992, Turbidite sandstones: AGIP, Istituto di geologia, Università di Parma. 275 p.

Natland, M.L., Gonzalez, P.E., Canon, A., and Ernst, M., 1974, A System of Stages for Correlation of Magallanes Basin Sediments: Geological Society of America, Memoir 139, 126 p.

Normark, W.R., 1970, Growth patterns of deep-sea fans: American Association of Petroleum Geologists, Bulletin, v. 54, no. 11, p. 2170-2195.

Pankhurst, R.J., Riley, T.R., Fanning, C.M., and Kelley, S.P., 2000, Episodic silicic volcanism in Patagonia and the Antarctic Peninsula: chronology of magmatism associated with the break-up of Gondwana: Journal of Petrology, v. 41, no. 5, p. 605-625.

Patacci, M., Haughton, P.D., and McCaffrey, W.D., 2015, Flow behavior of ponded turbidity currents: Journal of Sedimentary Research, v. 85, no. 8, p. 885-902.

Paull, C.K., Talling, P.J., Maier, K.L., Parsons, D., Xu, J., Caress, D.W., Gwiazda, R., Lundsten, E.M., Anderson, K., Barry, J.P., and Chaffey, M., 2018, Powerful turbidity currents driven by dense basal layers: Nature Communications, v. 9, no 1, p. 1-9.

Peakall, J., McCaffrey, B., and Kneller, B., 2000, A process model for the evolution, morphology, and architecture of sinuous submarine channels: Journal of Sedimentary Research, v. 70, no. 3, p. 434-448.

Piper, D.J., and Kontopoulos, N., 1994, Bed forms in submarine channels; comparison of ancient examples from Greece with studies of Recent turbidite systems: Journal of Sedimentary Research, v. 64, no. 2, p. 247-252.

Piper, D.J., and Normark, W.R., 1983, Turbidite depositional patterns and flow characteristics, Navy submarine fan, California Borderland: Sedimentology, v. 30, no. 5, p. 681-694.

Piper, D.J., Shor, A.N., Farre, J.A., O'Connell, S., and Jacobi, R., 1985, Sediment slides and turbidity currents on the Laurentian Fan: Sidescan sonar investigations near the epicenter of the 1929 Grand Banks earthquake: Geology, v. 13, no. 8, p. 538-541.

Pirmez, C., Beaubouef, R.T., Friedmann, S.J., and Mohrig, D.C., 2000, Equilibrium profile and baselevel in submarine channels: examples from Late Pleistocene systems and implications for the architecture of deepwater reservoirs, *in* Weimer, P., (ed.), Deep-Water Reservoirs of the World: 20th Annual Research Conference, Golf Coast Section, SEPM (Society for Sedimentary Geology), p. 782-805.

Posamentier, H.W., 2003, Depositional elements associated with a basin floor channel–levee system: case study from the Gulf of Mexico: Marine and Petroleum Geology, v. 20, no. 6-8, p. 677-690.

Postma, G., Nemec, W., and Kleinspehn, K.L., 1988, Large floating clasts in turbidites: a mechanism for their emplacement: Sedimentary Geology, v. 58, no. 1, p. 47-61.

Rees, A.I., 1968, The production of preferred orientation in a concentrated dispersion of elongated and flattened grains: The Journal of Geology, v. 76, no. 4, p. 457-465.

Rees, A.I., 1983, Experiments on the production of transverse grain alignment in a sheared dispersion: Sedimentology, v. 30, no. 3, p. 437-448.

Romans, B.W., Hubbard, S.M., and Graham, S.A., 2009, Stratigraphic evolution of an outcropping continental slope system, Tres Pasos Formation at Cerro Divisadero, Chile: Sedimentology, v. 56, no. 3, p. 737-764.

Romans, B.W., Fildani, A., Hubbard, S.M., Covault, J.A., Fosdick, J.C., and Graham, S.A., 2011, Evolution of deep-water stratigraphic architecture, Magallanes Basin, Chile: Marine and Petroleum Geology, v. 28, no. 3, p. 612-628.

Sánchez, G.J., Baptista, N., Parra, M., Montilla, L., Guzmán, O.J., and Finno, A., 2010, The Monagas Fold-Thrust belt of Eastern Venezuela. Part II: Structural and palaeo-geographic controls on the turbidite reservoir potential of the middle Miocene foreland sequence: Marine and Petroleum Geology, v. 28, no. 1, p. 70-80.

Scott, K.M., 1966, Sedimentology and dispersal pattern of a Cretaceous flysch sequence, Patagonian Andes, southern Chile: American Association of Petroleum Geologists, Bulletin, v. 50, no. 1, p. 72-107.

Shultz, M.R., Fildani, A., Cope, T.D., and Graham, S.A., 2005, Deposition and stratigraphic architecture of an outcropping ancient slope system: Tres Pasos Formation. Magallanes Basin, southern Chile, *in* Hodgson, D.M. and Flint, S.S., (eds.), Submarine Slope Systems: Processes and Products, Geological Society, London, Special Publication 244, p. 27-50.

Sickmann, Z.T., Schwartz, T.M., and Graham, S.A., 2018. Refining stratigraphy and tectonic history using detrital zircon maximum depositional age: an example from the Cerro Fortaleza Formation, Austral Basin, southern Patagonia: Basin Research, v. 30, no. 4, p. 708-729.

Smith, C.H.L., 1977, Sedimentology of the Late Cretaceous (Santonian-Maestrichtian) Tres Pasos Formation, Ultima Esperanza District, southern Chile [unpublished Master's thesis]: University of Wisconsin, Madison, U.S.A. 129 p.

Smith, R., and Joseph, P., 2004, Onlap stratal architectures in the Gres d'Annot: geometric models and controlling factors, *in* Joseph, P., and Lomas, S.A., (eds), Deep-Water Sedimentation in the Alpine Basin of SE France: New perspectives on the Grès d'Annot and related systems, Geological Society, London, Special Publication 221, no. 1, p. 389-399.

Smith, D.P., Ruiz, G., Kvitek, R., and Iampietro, P.J., 2005, Semiannual patterns of erosion and deposition in upper Monterey Canyon from serial multibeam bathymetry: Geological Society of America, Bulletin, v. 117, p. 1123-1133.

Sohn, Y.K., 2000, Depositional processes of submarine debris flows in the Miocene fan deltas, Pohang Basin, SE Korea with special reference to flow transformation: Journal of Sedimentary Research, v. 70, no. 3, p .491-503.

Sohn, Y.K., Choe, M.Y., and Jo, H.R., 2002, Transition from debris flow to hyperconcentrated flow in a submarine channel (the Cretaceous Cerro Toro Formation, southern Chile): Terra Nova, v. 14, no. 5, p. 405-415.

Soutter, E.L., Kane, I.A., Fuhrmann, A., Cumberpatch, Z.A., and Huuse, M., 2019, The stratigraphic evolution of onlap in siliciclastic deep-water systems: Autogenic modulation of allogenic signals: Journal of Sedimentary Research, v. 89, no. 10, p. 890-917.

Sprague, A.R.G., Sullivan, M.D., Campion, K.M., and Jensen, G.N., 2002, The physical stratigraphy of deep-water strata: A hierarchical approach to the analysis of genetically-related stratigraphic elements for improved reservoir prediction, *in* American Association of Petroleum Geologists Annual Meeting, Program with Abstracts, Houston, Texas, p. 167-167.

Sprague, A.R.G., Garfield, T.R., Goulding, F., Beaubouef, R.T., Sullivan, M.D., Rossen, C., Campion, K.M., Sickafoose, D.K., Abreu, V., Shellpeper, M.E., Jensen, G.N., Jennette, D. C., Pirmez, C., Dixon, B.T., Ying, D., Ardill, J.A., Mohrig, D.C., Porter, M.L., Farrell, M. E., and Mellere, D., 2005, Integrated slope channel depositional models: the key to successful prediction of reservoir presence and quality in offshore west Africa: Colegio de Ingenenieros Petroleros de México, cuarto E-Exitep, Veracruz, Mexico, p. 1-13.

Stanley, D.J., 1974, Pebbly mud transport in the head of Wilmington Canyon: Marine Geology, v. 16, p. M1-M8.

Stern, C.R., Mukasa, S.B., and Fuenzalida, P.R., 1992, Age and petrogenesis of the Sarmiento ophiolite complex of southern Chile: Journal of South American Earth Sciences, v. 6, no. 1-2, p. 97-104.

Stern, C.R., and de Wit, M.J., 2003, Rocas Verdes ophiolites, southernmost South America: Remnants of progressive stages of development of oceanic-type crust in a continental margin back-arc basin, *in* Dilek, Y., and Robinson, P.T., (eds.), Ophiolites in Earth History, Geological Society, London, Special Publication 218, no. 1, p. 665-683.

Stern, C.R., and Mukasa, S.B., 1992, Age and petrogenesis of the Sarmiento ophiolite complex of southern Chile: Journal of South American Earth Sciences, v. 6, no. 1-2, p. 97-104.

Stevenson, C.J., Talling, P.J., Masson, D.G., Sumner, E.J., Frenz, M., and Wynn, R.B., 2014, The spatial and temporal distribution of grain-size breaks in turbidites: Sedimentology, v. 61, no. 4, p. 1120-1156.

Stevenson, C.J., Jackson, C.A.L., Hodgson, D.M., Hubbard, S.M., and Eggenhuisen, J.T., 2015, Deep-water sediment bypass: Journal of Sedimentary Research, v. 85, no. 9, p. 1058-1081.

Straub, K.M., Mohrig, D., Buttles, J., McElroy, B., and Pirmez, C., 2011, Quantifying the influence of channel sinuosity on the depositional mechanics of channelized turbidity currents: A laboratory study: Marine and Petroleum Geology, v. 28, no. 3, p. 744–760.

Sullivan, M., Jensen, G., Goulding, F., Jennette, D., Foreman, L., and Stern, D., 2000, Architectural Analysis of Deep-Water Outcrops: Implications for Exploration and Development of the Diana Sub-Basin, Western Gulf of Mexico, *in* Weimer, P., (ed.), Deep-Water Reservoirs of the World: 20th Annual Research Conference, Gulf Coast Section, SEPM (Society for Sedimentary Geologists) [Society of Economic Paleontologists and Mineralogists], p. 1010-1031.

Talling, P.J., Masson, D.G., Sumner, E.J., and Malgesini, G., 2012, Subaqueous sediment density flows: Depositional processes and deposit types: Sedimentology, v. 59, no. 7, p. 1937-2003.

Tek, D.E., Poyatos-Moré, M., Patacci, M., McArthur, A.D., Colombera, L., Cullen, T.M., and McCaffrey, W.D., 2020, Syndepositional tectonics and mass-transport deposits control channelized, bathymetrically complex deep-water systems (Aínsa depocenter, Spain): Journal of Sedimentary Research, v. 90, no. 7, p. 729-762.

Tek, D.E., McArthur, A.D., Poyatos-Moré, M., Colombera, L., Patacci, M., Craven, B., and McCaffrey, W.D., 2021, Relating seafloor geomorphology to subsurface architecture: how mass-transport deposits and knickpoint-zones build the stratigraphy of the deep-water Hikurangi Channel: Sedimentology, v. 68, no. 7, p. 3141-3190.

Vendettuoli, D., Clare, M.A., Clarke, J.H., Vellinga, A., Hizzet, J., Hage, S., Cartigny, M.J.B., Talling, P.J., Waltham, D., Hubbard, S.M., and Stacey, C., 2019, Daily bathymetric surveys document how stratigraphy is built and its extreme incompleteness in submarine channels: Earth and Planetary Science Letters, v. 515, p. 231-247.

Walker, R.G., 1975, Generalized facies models for resedimented conglomerates of turbidite association: Geological Society of America, Bulletin, v. 86, no. 6, p. 737-748.

Walker, R.G., 1978, Deep-water sandstone facies and ancient submarine fans: models for exploration for stratigraphic traps: American Association of Petroleum Geologists Bulletin, v. 62, no. 6, p. 932-966.

Walker, R.G., 2006, Facies models revisited, *in* Posamentier, H.W., and Walker, R.G., (eds.), SEPM (Society for Sedimentary Geology), Special Publication 84, p. 1-17.

Wilson, T.J., 1991, Transition from back-arc to foreland basin development in the southernmost Andes: Stratigraphic record from the Ultima Esperanza District, Chile: Geological Society of America Bulletin, v. 103, no. 1, p. 98-111.

Winn, R.D.J., and Dott, R.H.J., 1977, Large-scale traction-produced structures in deep-water fan-channel conglomerates in southern Chile: Geology, v. 5, no. 1, p .41-44.

Winn, R.D.J., and Dott, R.H.J., 1979, Deep-water fan-channel conglomerates of Late Cretaceous age, southern Chile: Sedimentology, v. 26, no. 2, p. 203-228.

Wynn, R.B., Kenyon, N.H., Masson, D.G., Stow, D.A., and Weaver, P.P., 2002, Characterization and recognition of deep-water channel-lobe transition zones: American Association of Petroleum Geologists, Bulletin, v. 86, no. 8, p. 1441-1462.

FIGURES

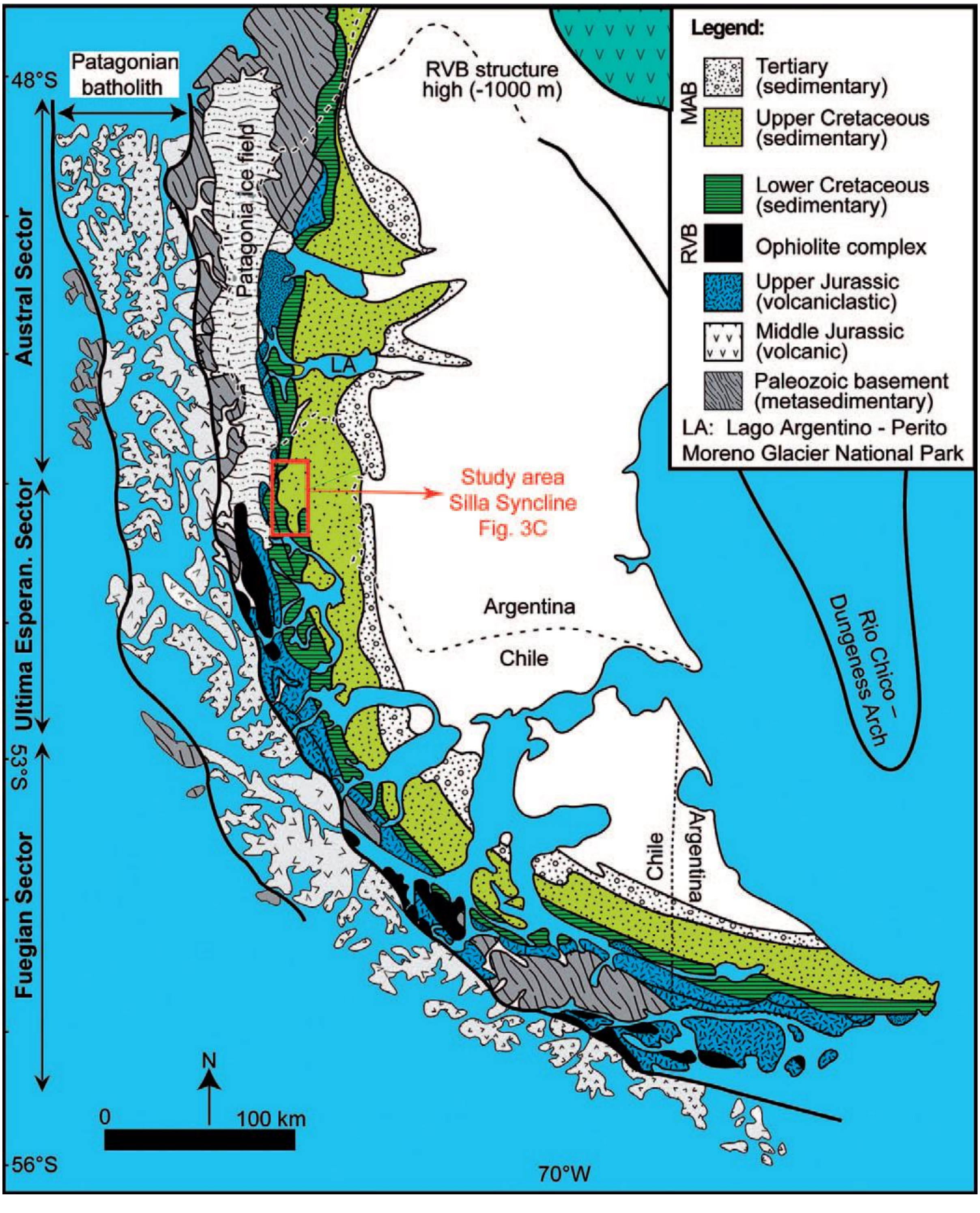

Figure 1. Regional geological map of the Magallanes–Austral (MA) foreland basin, with the key for the main geological units (modified from Malkowski et al. 2015). RVB-Rocas Verdes Basin.

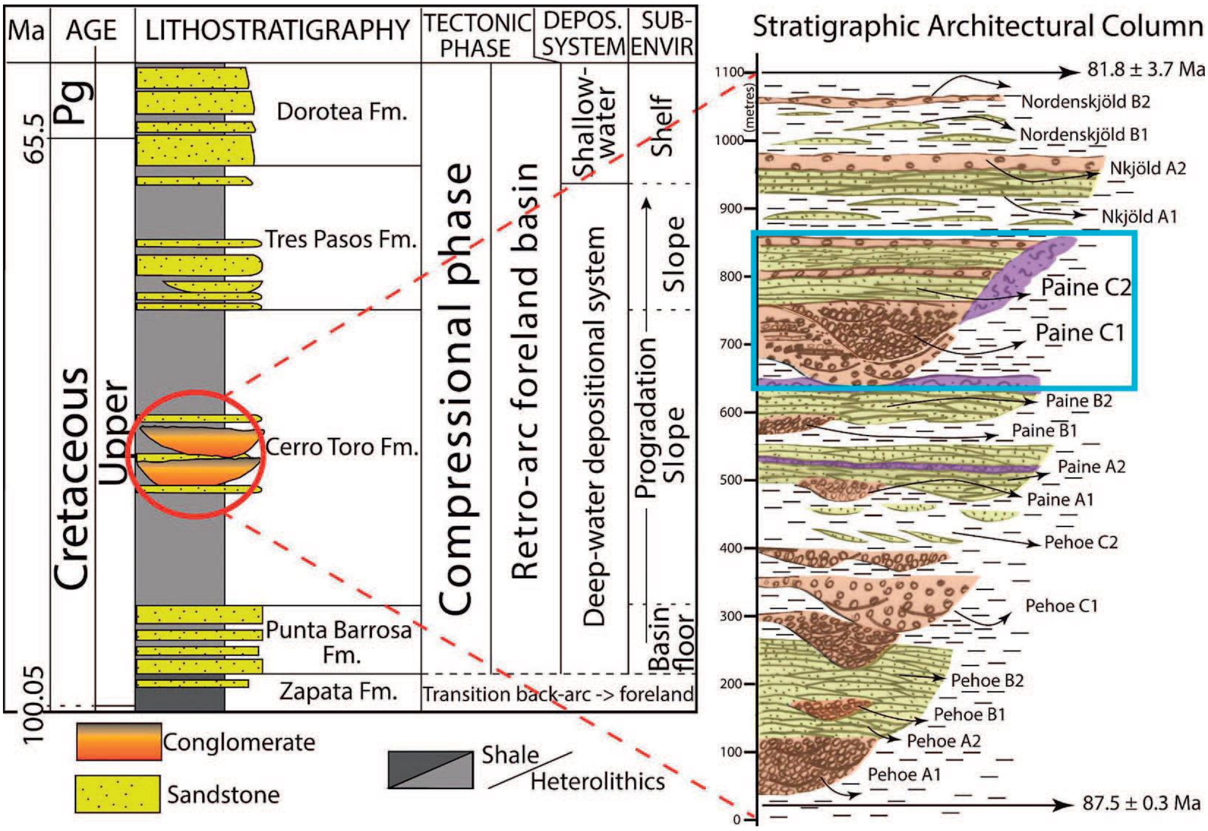

Figure 2. Generalized stratigraphic column for the Magallanes Basin, Ultima Esperanza District, southern Chile, and stratigraphic architectural column of the Silla Syncline area showing in the blue rectangle the studied deposits. Main lithostratigraphic formations, tectonic phases, depositional system and interpreted sub-environments are shown. Bozetti et al. (2018), modified after Romans et al. (2011), [originally adapted from Wilson (1991) and Fildani and Hessler (2005)]. Radiometric ages are from from Bernhardt et al., 2012.

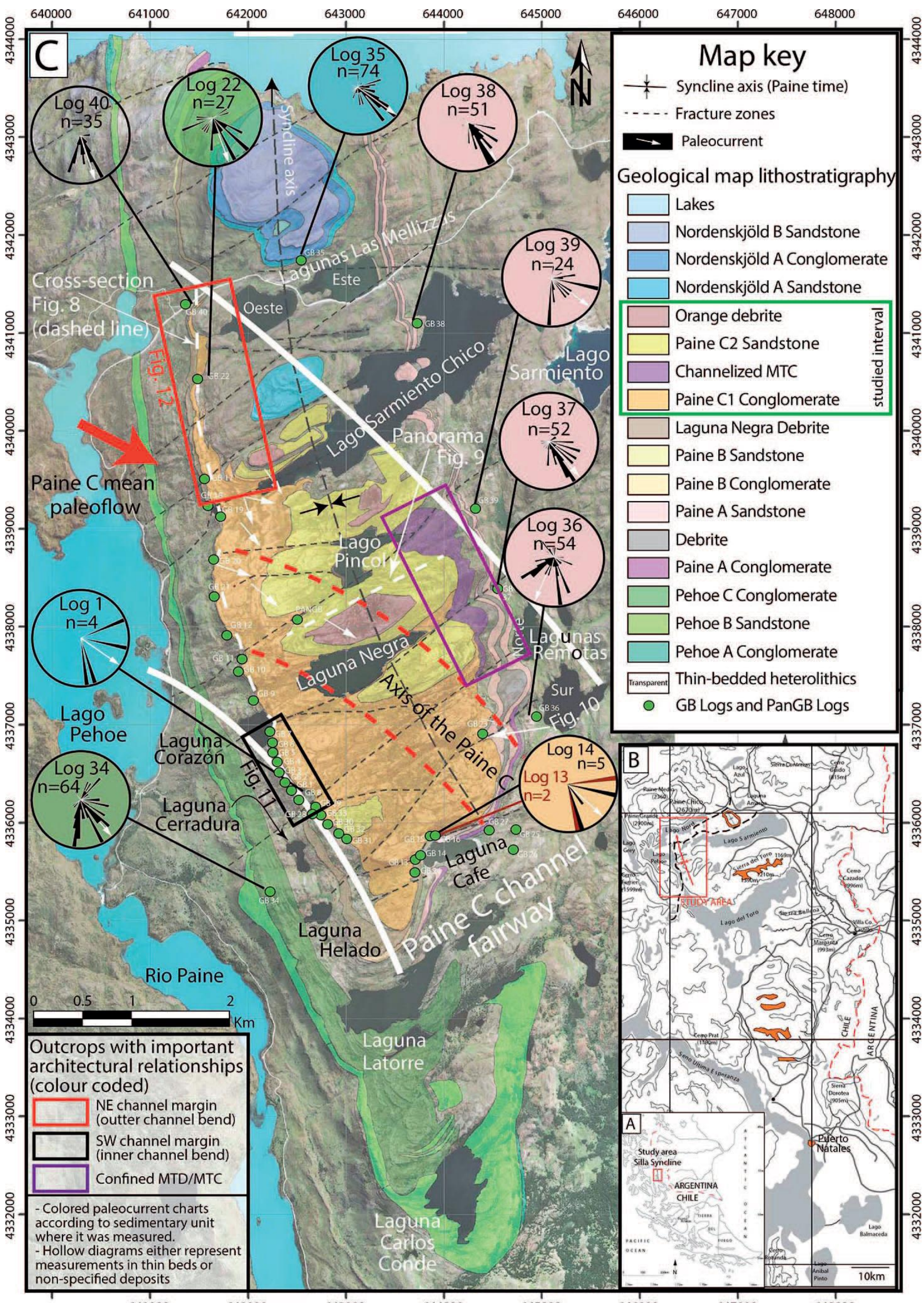

Figure 3. A) Principal localities around the field area, showing outcrops of the main Cerro Toro axial channel system (orange). B) Geological map of the field area, with interpreted the

Paine C channel system main boundary (white continuous line), based on the pinch-out of the channelized facies onto adjacent thin bedded facies, and interpreted channel axis boundary (red dashed line), representing the trend of the most amalgamated deposits, and deepest erosional cut of the channelized deposits into the underlying stratigraphy. Paleocurrent measurements (rose diagrams) are based dominantly on sole marks in conglomerates and sandstones (colors are as per map key, indicating the respective stratigraphic units in which they were measured). Colored rectangles indicate key localities used for defining facies associations (modified from Bozetti et al. 2018)

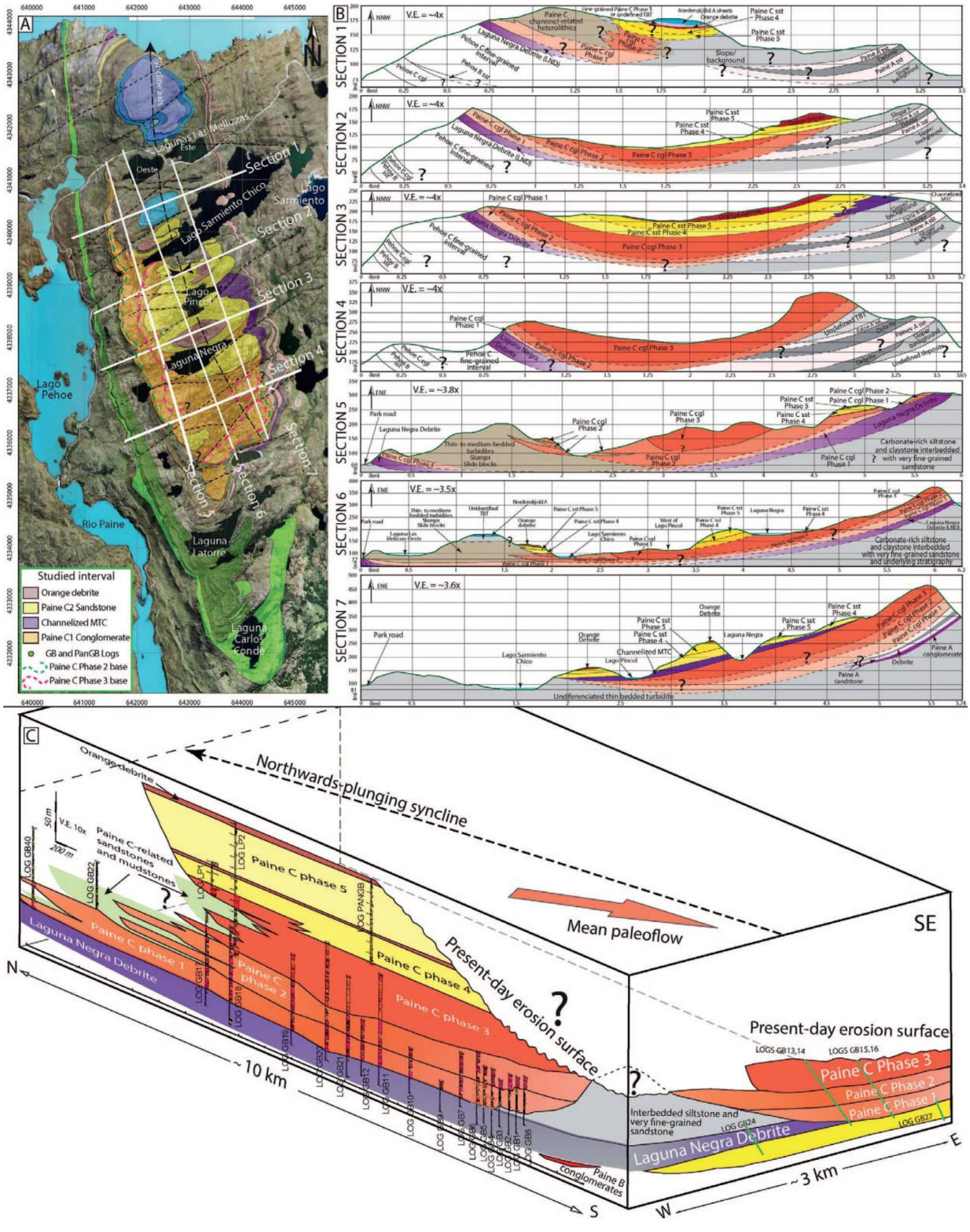

Figure 4. A) Geological map of the Silla Syncline area with map view of the sections in Part B. B) Cross sections of the Silla Syncline area, the same units related to the Paine C channel system. C) Composite cross section of the Paine C with restored regional structures, highlighting a section in the west limit of the outcrop, a transect interpreted based on the

combination of cross sections in Part B, and a section in the southernmost part of the outcrop belt.

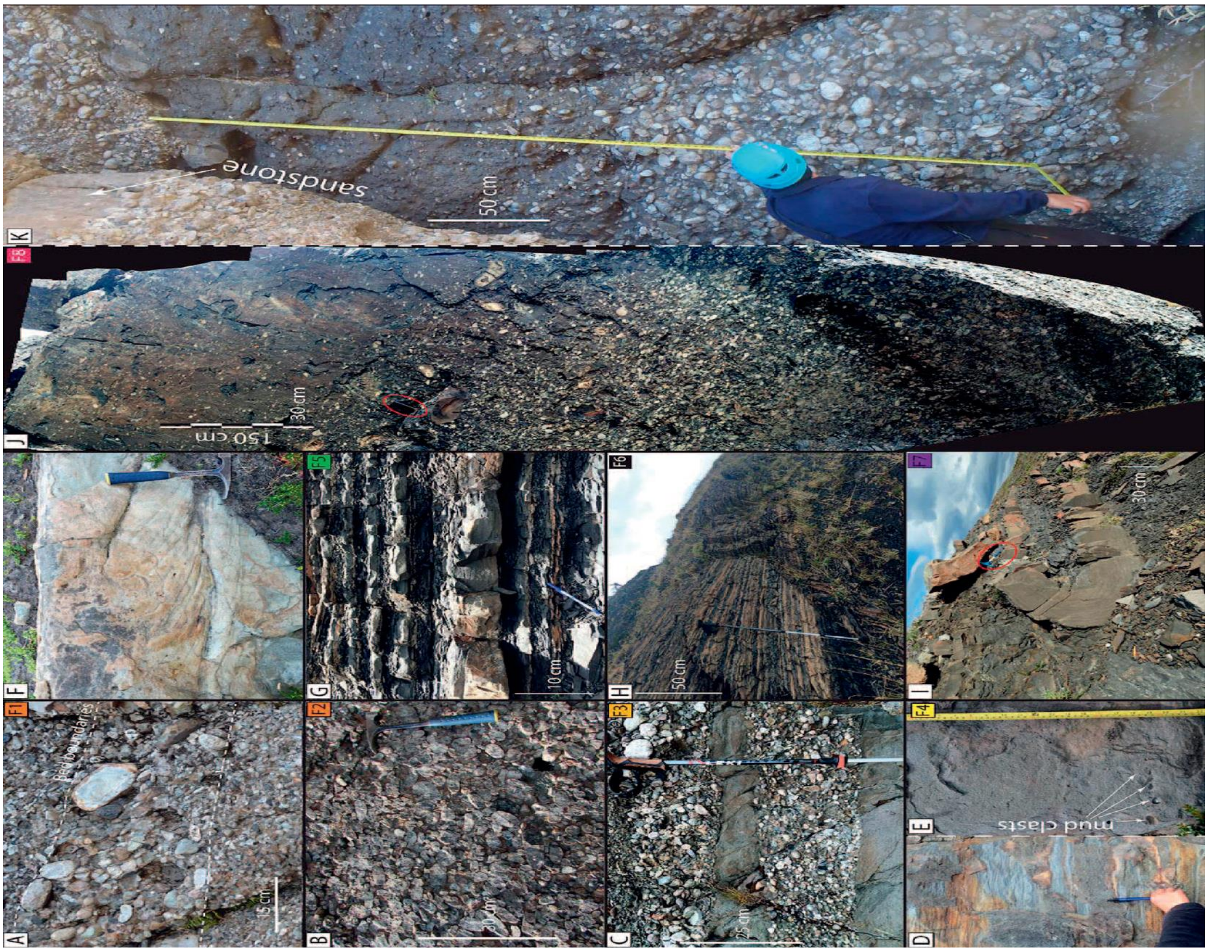

Figure 5. Facies scheme illustrating the seven main facies (modified from Bozetti et al. 2018). A) F1. Low matrix content, very large pebble to small cobble extraformational clast-supported conglomerate. B) F2. High-matrix-content pebble to small cobble extraformational clast-supported conglomerate. C) F3. Bipartite large to very large pebble-clast-supported conglomerate overlain by coarse to medium sandstone. D) F4. Medium-grained matrix-poor sandstone with dewatering structures throughout. E) F4. Coarse- to medium-grained more matrix-rich graded sandstone, with mud-clast horizon near the base. F) F5. Interbedded thin- to medium-bedded graded sandstones and mudstones. Sandstone grain size varies from medium at the base of thicker beds, to fine-grained at base of thin beds. G) F6. Thinly

laminated carbonate-rich silt and clay, with sparse very-fine-grained sandstones. H) F7. Slump-folded medium-grained sandstone in mud matrix, in an interval of interbedded graded sandstone to mudstone. I) F8. Transitional clast- to matrix-supported conglomerate, with size and number of extraformational clasts decreasing upwards, concentration of very large intraformational clasts and rafts in the lower part of matrix-supported interval. J) F8. Inversely to normally graded clast- to matrix-supported transitional conglomerate, overlain by a sandstone. See main text and Table 1 for facies description and interpretation.


(A)
fA 1
2 m
(B)
fA 2
1 m
Closer to the axis
(D)
fA 3
30 cm
Sand-filled
vertical
burrows
(Diplocraterion)
(C)
fA 2*
1m
Closer to the margin
(E)
fA 4
2 m
(F)
fA 5
2 m
(G)
fA 6
60 cm
(H)
fA 7
(I)
fA 8
1 m

Figure 6. Facies-associations scheme, illustrating the seven associations defined during the acquisition and processing of the data: (A) fA1: channel axis (UTM: 644023 m E, 4336628 m S); (B) fA2: channel off-axis near the axis (UTM: 641940 m E, 4337742 m S); (C) fA2*: channel off-axis near the margin (UTM: 4336739 m S, 642327 m E); (D) fA3: channel margin (UTM: 642472 m E, 4336422 m S); (E) fA4: amalgamated sandstone (UTM: 641914 m E, 4339487 m S); (F) fA5: non-amalgamated sandstone (UTM: 642763 m E, 4338120 m S); (G) fA6: terrace or internal levees (UTM: 641641 m E, 4340483 m S); (H) fA7: confined MTC (UTM: 644089 m E, 4339051 m S); (I) fA8: extrachannel deposits (UTM: 644206 m E, 4339150 m S).

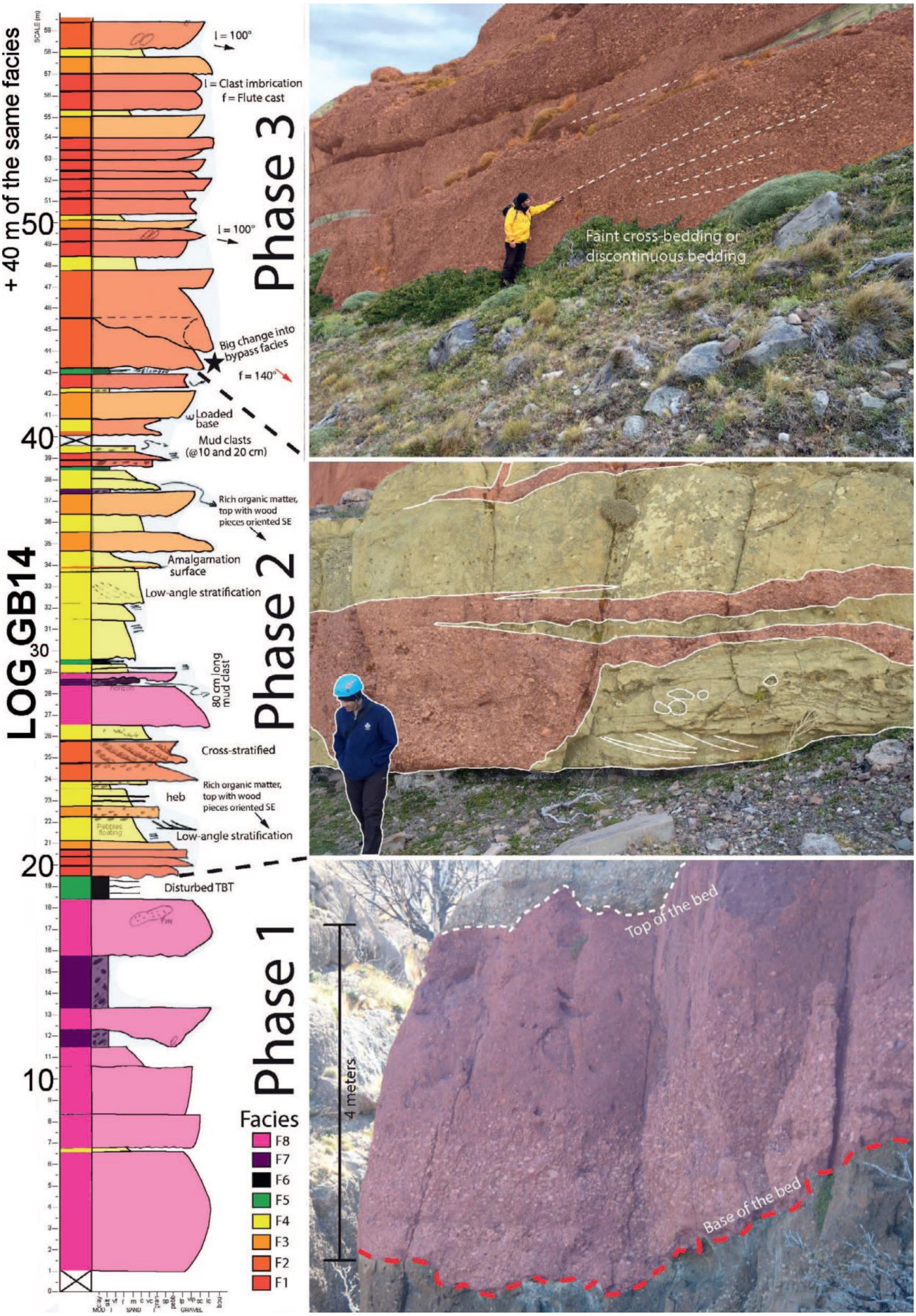
+ 40 m of the same facies
LOG GB14
SCALE (m)
I = 100°
I = Clast imbrication
f = Flute cast
Big change into bypass facies
f = 140°
Loaded base
Mud clasts (@10 and 20 cm)
Rich organic matter, top with wood pieces oriented SE
Amalgamation surface
Low-angle stratification
80 cm long mud clast
Cross-stratified
heb
Pebbles floating
Disturbed TBT
Facies
F8
F7
F6
F5
F4
F3
F2
F1
clay
silt
vf
f
m
c
vc
gp
ip
vp
sc
lc
bou
MUD
SAND
GRAVEL
Phase 3
Phase 2
Phase 1
Faint cross-bedding or discontinuous bedding
Top of the bed
Base of the bed
4 meters

Figure 7. Sedimentary log GB14 (see Fig. 3 for location) placed next to three outcrop photographs that illustrate the main facies and their stacking pattern in each of the three phases of the Paine C lower unit. Phase 1 is highly aggradational, composed dominantly of facies F8 conglomerates; Phase 2 records a substantial amount of sandstones (F4) and clast-supported conglomerates (F1, F2, F3), but also preserves some F8; Phase 3 is made dominantly of clast-supported conglomerate (F1, F2), with a small amount of lenticular sandstones (F3, F4). See Fig. 5, Table 1, and the main text for facies details.

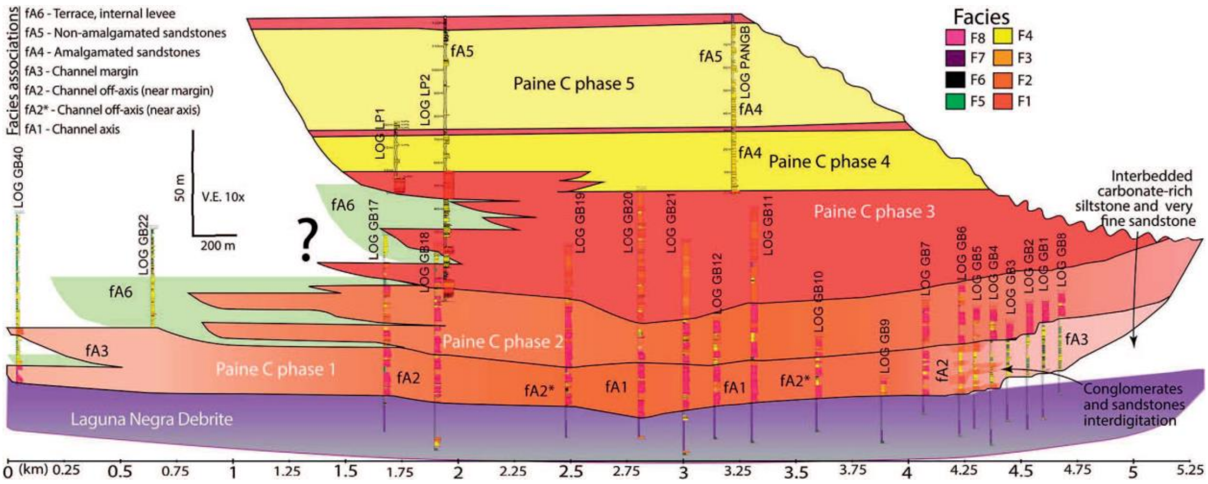

Figure 8. Paine C log correlation of the lower conglomeratic unit, on the western limb of the Silla Syncline (Fig. 3). Note that this is a highly oblique section across the 3.5 – 4-km-wide channel belt. Three phases are recognized based on sedimentary logs from across the syncline and on mapping data. Phases are individually explained in Fig. 7. Individual beds can be traced for hundreds of meters. However, amalgamation in the channel axis makes single bed correlation unreliable.

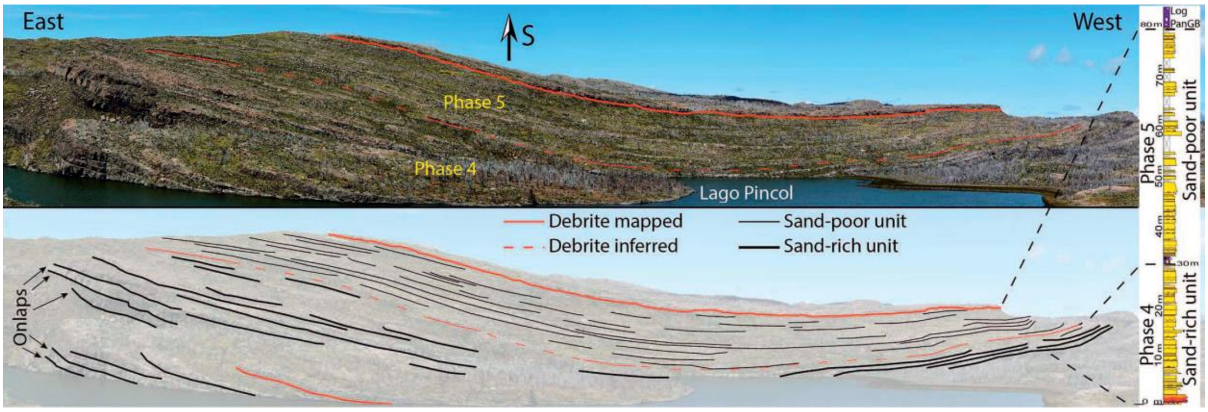

Figure 9. Section illustrating the difference between the amalgamated and the non-amalgamated packages of sandstones (see Fig. 3 for location). The poorly exposed areas probably represent concentration of fine-grained deposits. Though the beds in the upper package are typically non-amalgamated, some packages are still laterally continuous and can be traced across several hundreds of meters, occasionally across the entire outcrop-belt.

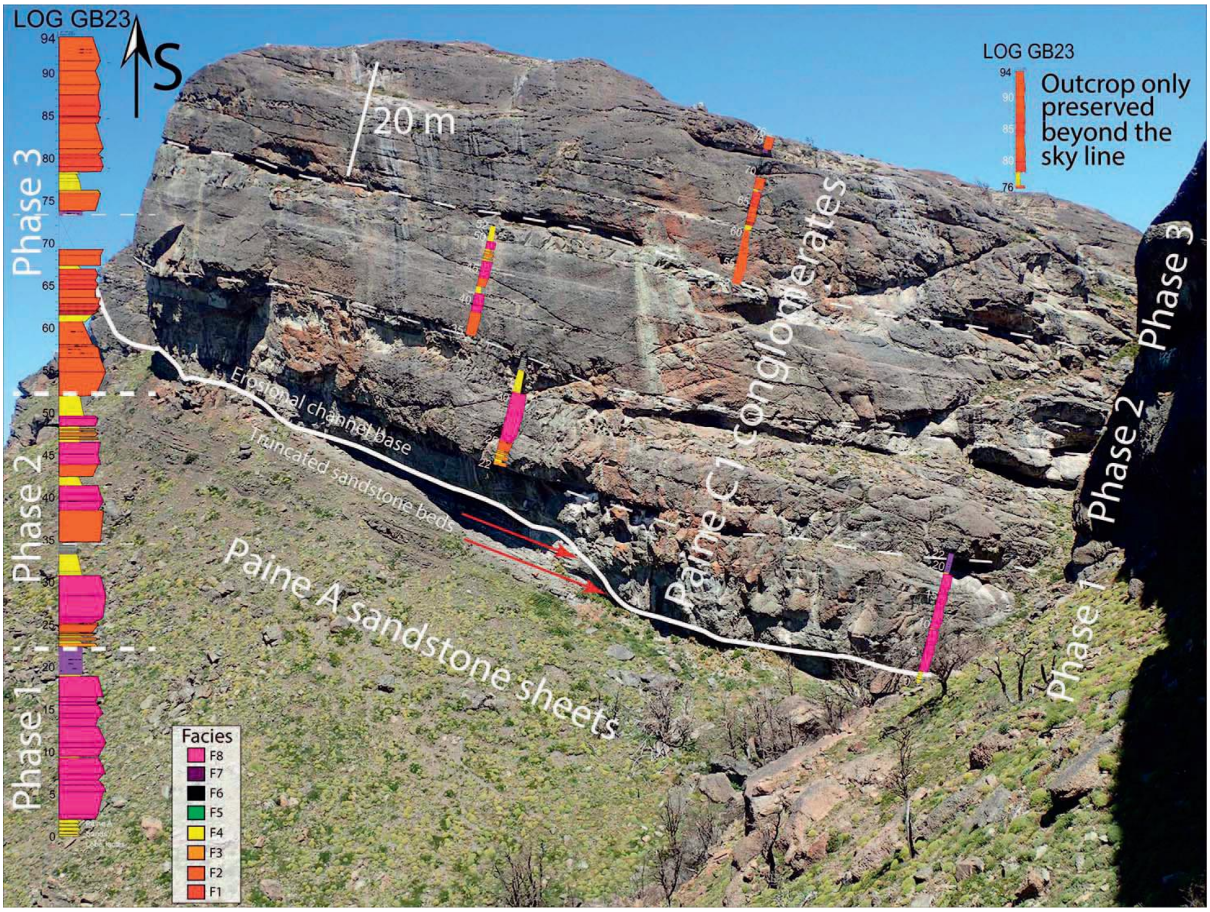

Figure 10. Image of the Paine C channel axis at the SE part of the Silla Syncline, with the sedimentary log GB23 draped on it, and continuously displayed on the left-hand side of the

figure. It records the thickest accumulation of gravelly deposits in the entire field area; more than 100 meters of dominantly conglomeratic deposits amalgamate in three distinct phases (phases 1 to 3), separated by intervals of partially disturbed sandstone + mudstone heterolithic deposits. See Fig. 7 for full description of the three phases and Fig. 3 for location.

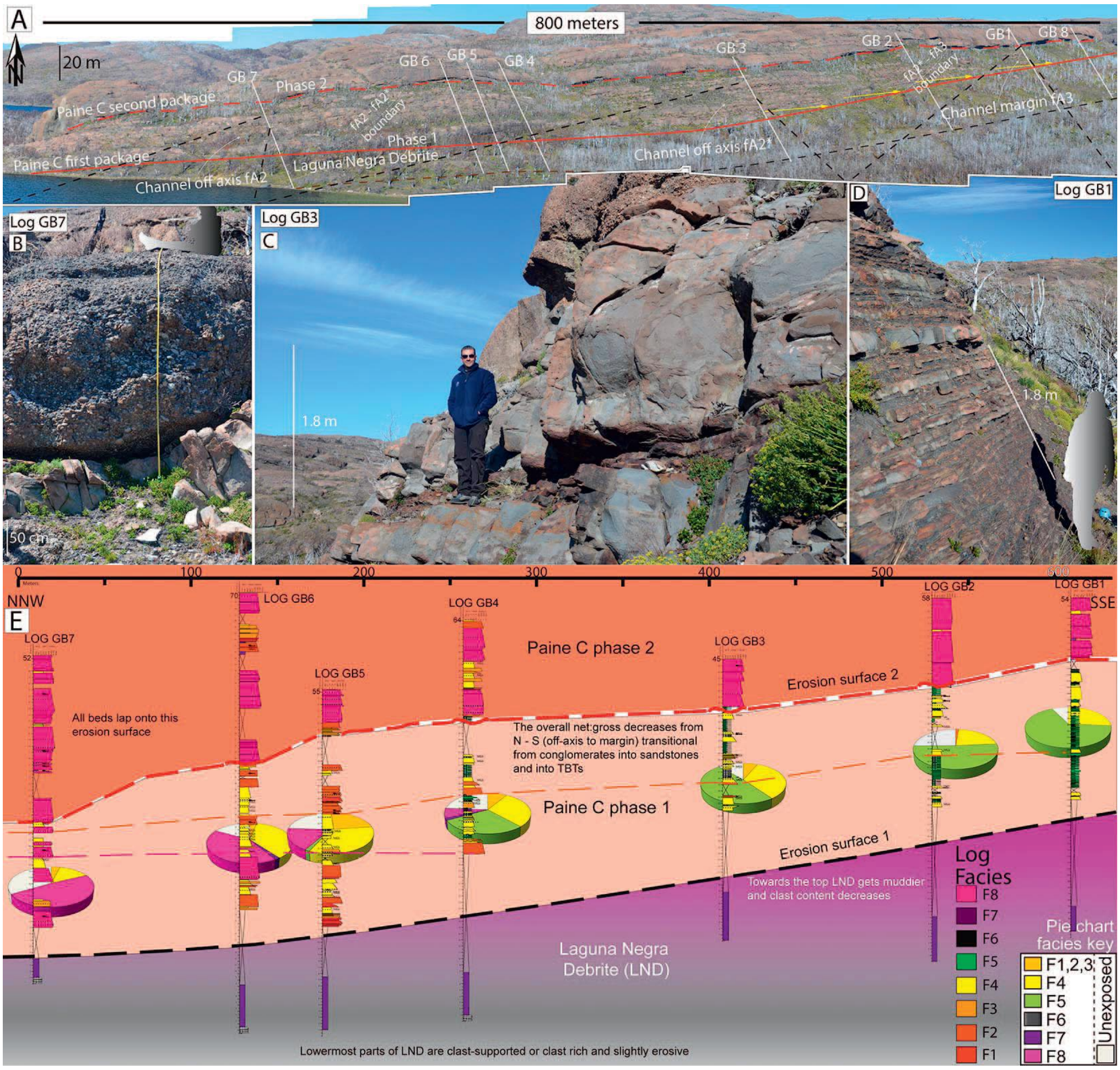

Figure 11. A) Photomosaic with some line interpretation of the western channel margin, at logs GB1 to GB8 location (see Fig. 3 for reference). Three detailed pictures show dominant facies at three different locations, highlighting the lateral facies variation. Note that the section is highly oblique, nonetheless the lateral transition is real, and represents the change from (B) axis or off-axis facies in Log GB7, into more (C) off-axis facies in Log GB3, ending

in (D) marginal facies at Log GB1 location (Figs. 3, 8). This transition happens in the first phase of channel entrenchment of the Paine C, which is later eroded into by Phase 2 (dashed red line in the panorama). Between the end of the deposition of the Phase 1 and erosion of the Phase 2, a continuous package of disturbed heterolithics occurs, being interpreted to represent “calm” time between erosion and aggradation of the phase 2. E) Log correlation from Logs GB1 to GB7, Log 1 being the most marginal and the Log GB7 the most axial, but still in the off-axis domain. The logs are also combined with pie charts. Facies 6 is absent in these logs. The pie charts represent the interval of interest, the one where the lateral facies variation is clear.

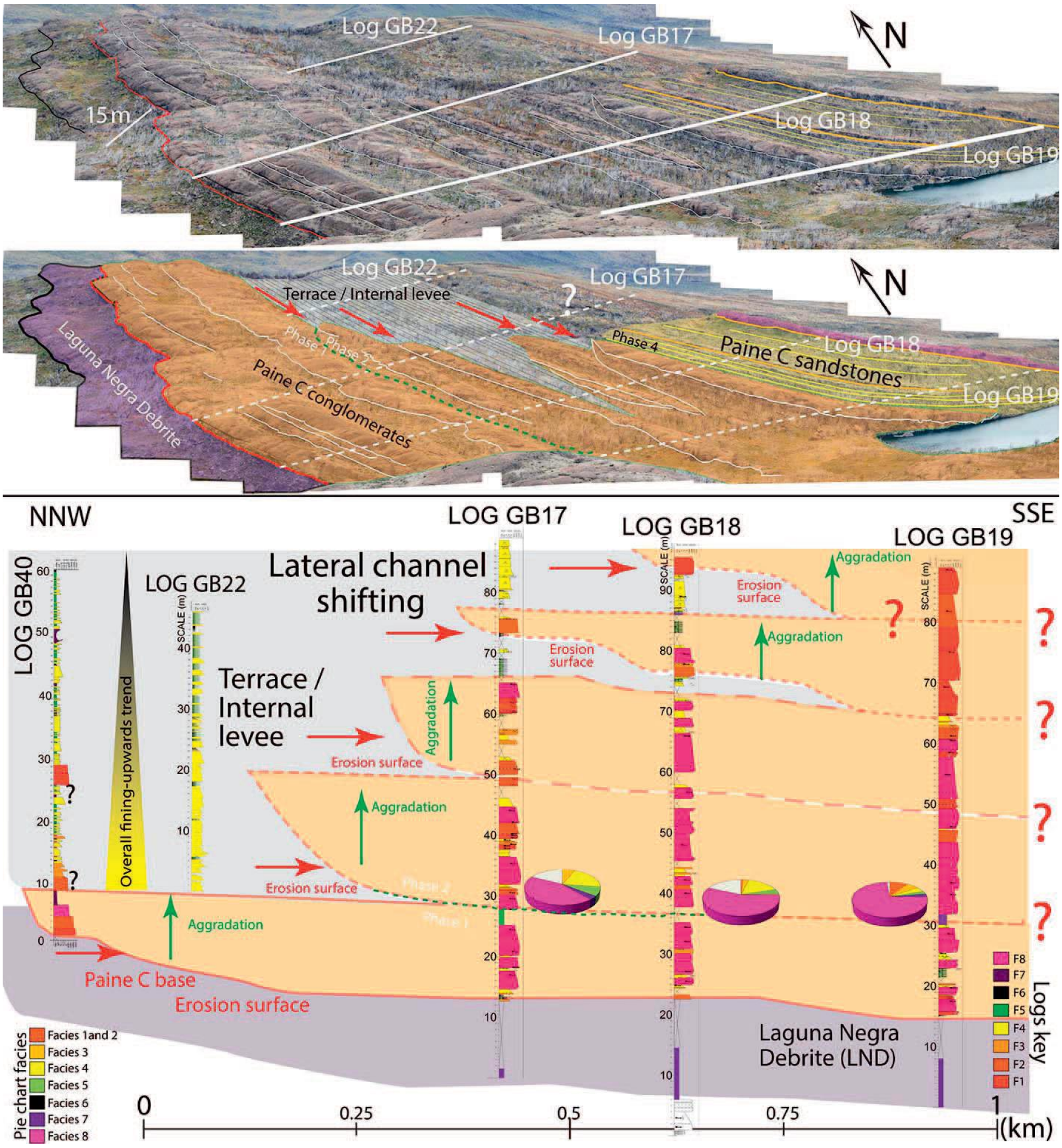

Figure 12. Interpreted photomosaic of the NE channel margin with a diagram showing the southwards lateral shift of the channel margin (see Fig. 3 for location). Three sedimentary logs across channelized deposits, and one recording deposits immediately lateral to them, record repeated intervals of erosion and aggradation (illustrated by red and green arrows). Note that this channel margin does not have the lateral facies transition recorded in the SW channel margin (Fig. 11).

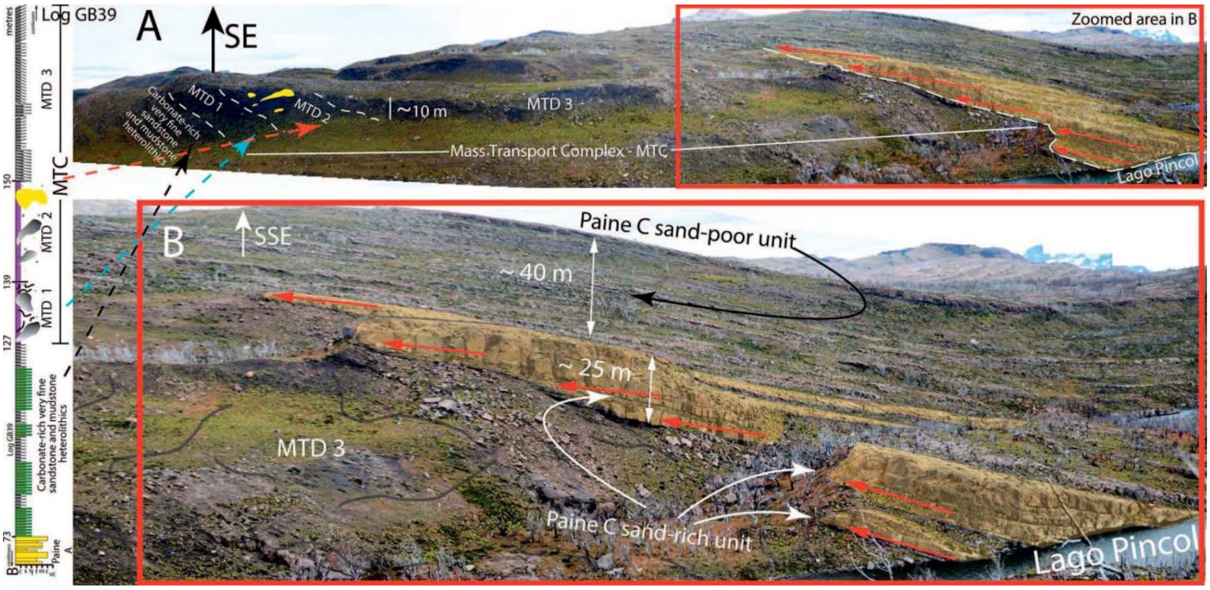

Figure 13. Channelized mass-transport complex (MTC) outcrop (eastern limb of the syncline; see Fig. 3 for location), showing its three main mass-transport deposits (MTD) recognized in a generalized measured section. Sandstones of the upper part of the Paine C are observed at this outcrop to lap out onto the MTD 3. The interpretation of the confinement of the MTD is based on its restricted mapped area and stratigraphic association with the confined deposits of the Paine C. In Part B it is also possible to see the difference of the two phases of Paine C amalgamated and non-amalgamated sandstones (Fig. 9).

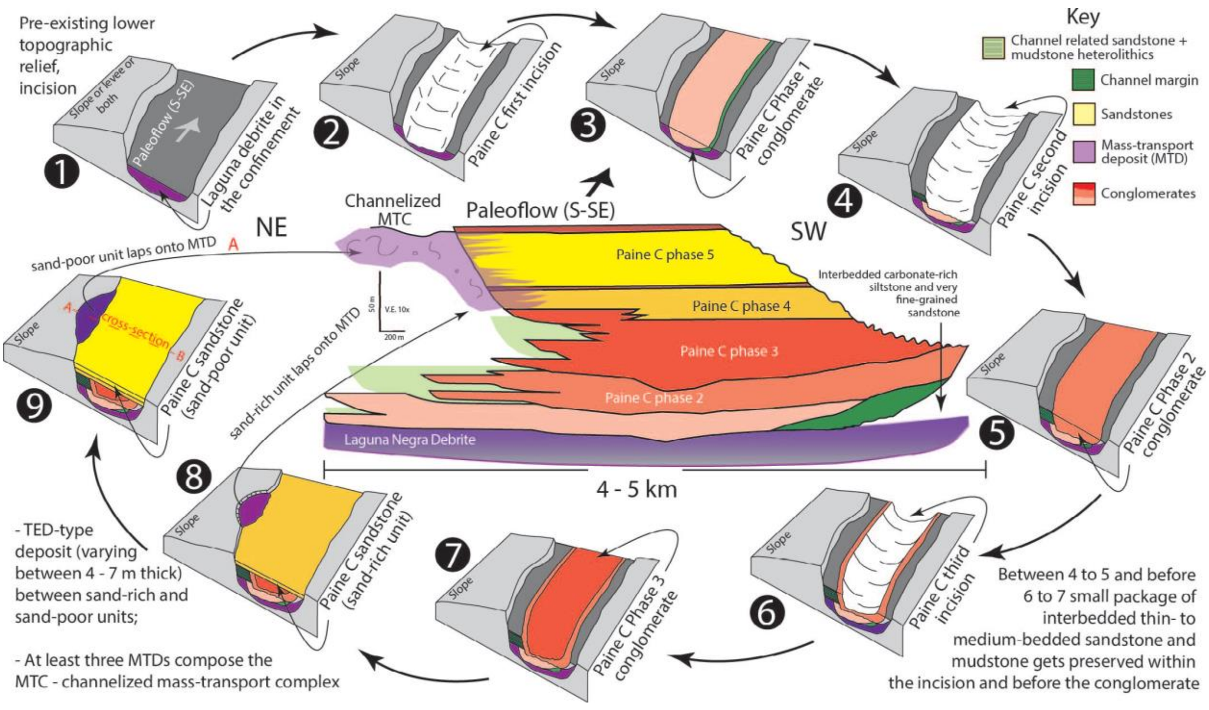

Figure 14. Synthesis of evolution of the Paine C channel system. 1) Deposition of the Laguna Negra Debrite within pre-existing low topographic relief (e.g., channel); 2) incision of the first phase of the Paine C; 3) infill of Paine C phase 1 with deposits dominantly conglomeratic, showing evident lateral facies transition from channel axis through off-axis and channel margin; 4) reincision of Paine C in its phase 2; 5) Infill of Paine C phase 2, which occurred in a series of erosion and aggradation events, shifting the channel towards the south, and depositing a package of intrachannel sandstone to mudstone heterolithics laterally to the coarse-grained deposits of the NE channel margin at this phase; 6) reincision of Paine C in its phase 3; 7) Infill of Paine C phase 3, which is the narrowest and the one recording most amalgamated conglomerates, interpreted as sediment-bypass-dominated; 8) deposit of the amalgamated sandstones package (Paine C phase 4), which occurred concomitantly with lower MTD of the channelized MTC in which the sandstones lap out onto; this phase marks a major change in channel architecture; 9) deposit of the non-amalgamated sandstones package (Paine C Phase 5), which also occurred simultaneously with upper MTD of the channelized MTC onto which the sandstones and mudstones lap out. The evolution of this phase from previous marks an overall fining- and thinning-upwards trend.

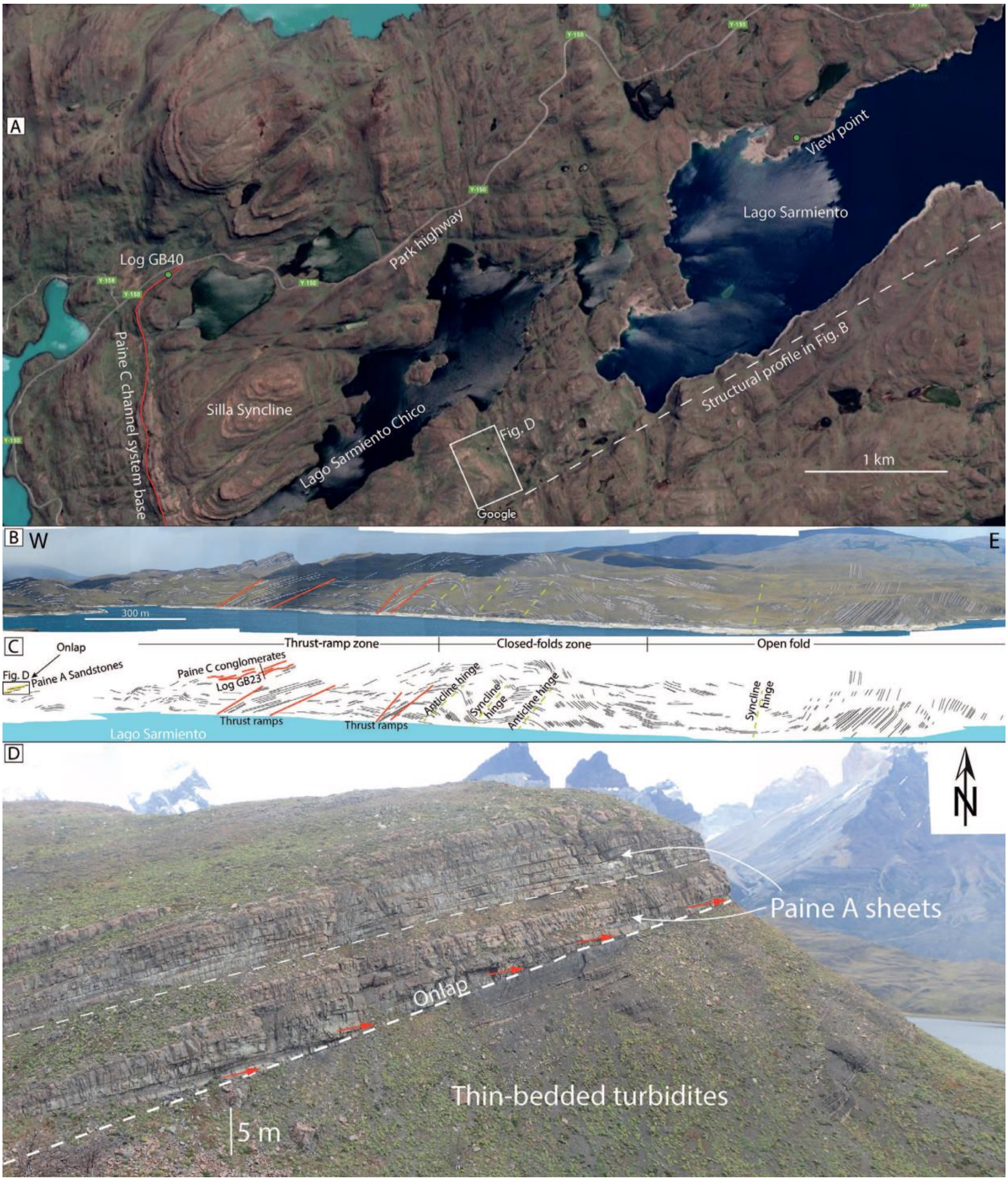

Figure 15. Complex structural profile of the area to the East of the outcrop belt. A) zoomed area to the north and northeast of the field area showing the area where profile in Parts B and C was acquired; B, C) structural profile illustrated and interpreted. D) Coarse-grained sediments of the Paine A onlapping fine-grained dominated deposits interpreted as slope sediments.

Table 1. Simplified facies scheme for the deposits encountered in the Paine C channel system and previously proposed facies equivalent.

<table>
<tr><th></th><th>Facies name</th><th>Description</th><th>Crane and Lowe 2008</th><th>Hubbard et al. 2008</th><th>Bernhardt et al. 2011</th></tr>
<tr><td>F1</td><td>Clast-supported conglomerate with low matrix content</td><td>Very large pebble to large cobble clast-supported highly amalgamated conglomerate, with 20 to 30% sandy matrix. a-parallel clast-imbrication common.</td><td rowspan="2">IIIcgl</td><td rowspan="2">IIIscg</td><td rowspan="2">Lf4</td></tr>
<tr><td>F2</td><td>Clast-supported conglomerate with high matrix content</td><td>Moderately to well-sorted pebble- to cobble-clast-supported conglomerate, with 25 to 40% sandy matrix, interstratified with sandstone.</td></tr>
<tr><td>F3</td><td>Bipartite conglomerate and sandstone couplet</td><td>Bipartite beds of clast-supported, pebble to cobble conglomerate, overlain via diffuse or sharp contact by fine to very coarse sandstone, commonly with traction structures.</td><td>IIIcgl overlain by IIIss</td><td>IIIscg overlain by IIIss</td><td>Lf4 overlain by Lf3</td></tr>
<tr><td>F4</td><td>Sandstone</td><td>Sharp-based very fine to very coarse highly amalgamated sandstones. Dominantly structureless, but may contain dewatering structures, ripple and parallel horizontal lamination, and trough cross-bedding.</td><td>~IIIss</td><td>IIIss</td><td>Lf3</td></tr>
<tr><td>F5</td><td>Graded sandstone to mudstone</td><td>Graded couplets of sandstone (usually c. 40% of the bed) and mudstone, some with Ta-e. May show multiple current orientations within the same bed.</td><td>IIImd-ss</td><td rowspan="2">IIIsm</td><td>Lf2</td></tr>
<tr><td>F6</td><td>Laminated carbonate-rich siltstone and claystone</td><td>Massive siltstone often interbanded with thinly laminated carbonate-rich siltstone and claystone.</td><td>IIImd</td><td>Lf1</td></tr>
<tr><td>F7</td><td>Debrites, mass-transport deposits (MTDs)</td><td>Pebbly mudstone, pebbly sandstone, matrix-supported conglomerate, slumps and slide blocks, ranging from slightly disturbed to completely chaotic, with intraclasts ranging up to few meters across.</td><td rowspan="2">IIIdia</td><td>IIIch</td><td>Lf6</td></tr>
<tr><td>F8</td><td>Transitional event deposits (TEDs)</td><td>Erosionaly based conglomerates, with clast-supported base, upward-increasing matrix (≤ 90%) both clasts and matrix commonly normally graded, mostly overlain by graded sandstone to mudstone.</td><td>IIImcg</td><td>Lf5 in part, with enclaves of Lf6</td></tr>
</table>

Table 2. Average facies distribution in the facies associations and/or architectural elements recognised in the Paine C channel system. Note that facies association 7 (#) is 100% composed of facies 6 deposits (e.g., slumps, debrites), which is itself composed of remobilized facies F4 (20%), F5 (30%), F6 (25%) and F8 (25%).

	fA1	**fA2**	**fA2***	**fA3**	**fA4**	**fA5**	**fA6**	**fA7**	**fA8**
name	Channel Axis	Channel off-axis close to axis	Channel off-axis close to margin	Channel margin	Bypass dominated sandstones	Aggradation dominated sandstones	Terrace, Internal levee	Confined MTD	Slope, External levee
F1	25%	10%	5%	0%	0%	0%	0%	0%	0%
F2	20%	15%	10%	0%	0%	0%	0%	0%	0%
F3	5%	20%	10%	0%	5%	1.25%	2.5%	0%	0%
F4	10%	10%	35%	15%	67.5%	43.75%	35%	20%	1.25%
F5	2.5%	7.5%	15%	72.5%	17.5%	50%	52.5%	30%	3.75%
F6	0%	0%	0	0%	0%	0%	0%	25%	90%
F7	7.5%	5%	5%	12.5%	10%	5%	10%	**100%**[#]	5%
F8	30%	32.5%	20%	0%	0%	0%	0%	25%	0%